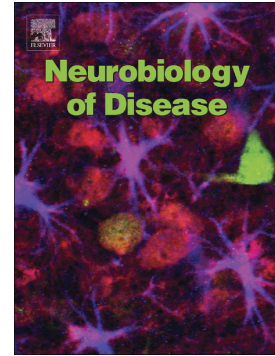


Accepted Manuscript

Hyperhomocysteinemia leads to exacerbation of ischemic brain damage: Role of GluN2A NMDA receptors

Ankur Jindal, Sathyanarayanan Rajagopal, Lucas Winter, Joshua W. Miller, Donald W. Jacobsen, Jonathan Brigman, Andrea M. Allan, Surojit Paul, Ranjana Poddar



PII: S0969-9961(18)30325-5
DOI: <https://doi.org/10.1016/j.nbd.2019.03.012>
Reference: YNBDI 4424
To appear in: *Neurobiology of Disease*
Received date: 26 July 2018
Revised date: 19 February 2019
Accepted date: 14 March 2019

Please cite this article as: A. Jindal, S. Rajagopal, L. Winter, et al., Hyperhomocysteinemia leads to exacerbation of ischemic brain damage: Role of GluN2A NMDA receptors, *Neurobiology of Disease*, <https://doi.org/10.1016/j.nbd.2019.03.012>

This is a PDF file of an unedited manuscript that has been accepted for publication. As a service to our customers we are providing this early version of the manuscript. The manuscript will undergo copyediting, typesetting, and review of the resulting proof before it is published in its final form. Please note that during the production process errors may be discovered which could affect the content, and all legal disclaimers that apply to the journal pertain.

**Hyperhomocysteinemia leads to exacerbation of ischemic brain damage: role of GluN2A
NMDA receptors**

Ankur Jindal*, Sathyanarayanan Rajagopal*, Lucas Winter*, Joshua W Miller[#], Donald W
Jacobsen[§], Jonathan Brigman[¶], Andrea M Allan[¶], Surojit Paul* and Ranjana Poddar*

*Department of Neurology, [¶]Department of Neurosciences, University of New Mexico Health
Sciences Center, 1 University of New Mexico, Albuquerque, NM – 87131

[#]Department of Nutritional Sciences, Rutgers University, 65 Dudley Road, Room 107
New Brunswick, NJ 08901

[§]Department of Cellular and Molecular Medicine, Lerner Research Institute, Cleveland Clinic,
Cleveland, OH 44195

[¶]Corresponding Author:

Ranjana Poddar, PhD, University of New Mexico Health Sciences Center, Department of
Neurology, 1, University of New Mexico, Albuquerque, NM – 87131

Tel: (505) 272-5859

e-mail: rpoddar@salud.unm.edu

Abbreviated title: Hyperhomocysteinemia and GluN2A-NMDAR in stroke injury

ABSTRACT

Hyperhomocysteinemia has been implicated in several neurodegenerative disorders including ischemic stroke. However, the pathological consequences of ischemic insult in individuals predisposed to hyperhomocysteinemia and the associated etiology are unknown. In this study, we evaluated the outcome of transient ischemic stroke in a rodent model of hyperhomocysteinemia, developed by subcutaneous implantation of osmotic pumps containing L-homocysteine into male Wistar rats. Our findings show a 42.3% mortality rate in hyperhomocysteinemic rats as compared to 7.7% in control rats. Magnetic resonance imaging of the brain in the surviving rats shows that mild hyperhomocysteinemia leads to exacerbation of ischemic injury within 24h, which remains elevated over time. Behavioral studies further demonstrate significant deficit in sensorimotor functions in hyperhomocysteinemic rats compared to control rats. Using pharmacological inhibitors targeting the NMDAR subtypes, the study further demonstrates that inhibition of GluN2A-containing NMDARs significantly reduces ischemic brain damage in hyperhomocysteinemic rats but not in control rats, indicating that hyperhomocysteinemia-mediated exacerbation of ischemic brain injury involves GluN2A-NMDAR signaling. Complementary studies in GluN2A-knockout mice show that in the absence of GluN2A-NMDARs, hyperhomocysteinemia-associated exacerbation of ischemic brain injury is blocked, confirming that GluN2A-NMDAR activation is a critical determinant of the severity of ischemic damage under hyperhomocysteinemic conditions. Furthermore, at the molecular level we observe GluN2A-NMDAR dependent sustained increase in ERK MAPK phosphorylation under hyperhomocysteinemic condition that has been shown to be involved in homocysteine-induced neurotoxicity. Taken together, the findings show that

hyperhomocysteinemia triggers an unique signaling pathway that in conjunction with ischemia-induced pathways enhance the pathology of stroke under hyperhomocysteinemic conditions.

Key words: hyperhomocysteinemia; GluN2A-NMDA receptors (also known as NR2A-NMDA receptors); GluN2B-NMDA receptors (also known as NR2B-NMDA receptors); ERK MAPK, GluN2A-NMDAR knockout mice; middle cerebral artery occlusion; ischemic brain injury; magnetic resonance imaging; behavioral studies;

ACCEPTED MANUSCRIPT

Abbreviations: NMDAR, N-methyl-D-aspartate receptors; ERK MAPK, extracellular-regulated kinase mitogen activated protein kinase; GluN2A-KO, GluN2A-NMDAR knockout mice, WT, wild type; MCAO, middle cerebral artery occlusion; MRI, magnetic resonance imaging; ADC, apparent diffusion coefficient; FA, fractional anisotropy;

ACCEPTED MANUSCRIPT

INTRODUCTION

Cerebral ischemic stroke is one of the leading causes of death and long-term disability worldwide (Chin and Vora, 2014; Johnston et al., 2009). Prevalence of comorbidities further worsen the clinical outcome, creating additional complications to any treatment approach for stroke (Fisher et al., 2009). A better understanding of stroke pathology under comorbid conditions is therefore of paramount importance to develop treatment strategies to reduce both stroke-induced brain damage as well as the synergistic effect induced by comorbid conditions.

Hyperhomocysteinemia, a common metabolic disorder characterized by systemic elevation of homocysteine is considered to be a risk factor for neurological disorders including ischemic stroke (Hankey and Eikelboom, 2001; Seshadri et al., 2002; Zoccolella et al., 2006). Epidemiological studies have linked mild (15-30 μM) and moderate (30-100 μM) hyperhomocysteinemia to nutritional deficiency of folate, vitamin B12 and vitamin B6, renal impairment and hypothyroidism, while severe hyperhomocysteinemic conditions (100-500 μM) are caused by genetic mutations and impaired activity of key enzymes in the homocysteine metabolic pathway (Austin et al., 2004; Obeid and Herrmann, 2006; Refsum et al., 1998; Seshadri et al., 2002). Although vitamin supplementation has considerably reduced mild to moderate hyperhomocysteinemia in the general population, the prevalence of hyperhomocysteinemia in the elderly population is still significantly high worldwide (Janson et al., 2002; Ramos et al., 2005; Robles et al., 2005; Selhub et al., 1999). This has been attributed to low nutritional absorption of essential B-vitamins, decreased metabolic function with advanced age, insufficient renal / hepatic function and medications involving vitamin B6 and folate antagonists (Hankey and Eikelboom, 2001; McCully, 2007; Refsum et al., 1998; Zoccolella et

al., 2006). Thus, it is conceivable that predisposition to hyperhomocysteinemia could contribute, at least in part, to the severity of neurological disorders in the elderly. However, the outcome of an ischemic insult under hyperhomocysteinemic conditions is still elusive.

In previous studies, we and others have reported that homocysteine is an agonist of the N-methyl-D-aspartate subtype of glutamate receptors (NMDARs) that is known to be involved in excitotoxicity and ischemic brain damage, caused by excessive release of glutamate during an insult (Ganapathy et al., 2011; Jara-Prado et al., 2003; Kruman et al., 2000; Lipton et al., 1997; Poddar and Paul, 2009; Poddar and Paul, 2013). Our recent findings also show that treatment of cultured neurons with homocysteine leads to cell death through activation of a unique signaling cascade, which is independent of excitotoxic cell death mediated through GluN2B subunit containing NMDARs (GluN2B-NMDAR), suggesting a role of GluN2A subunit containing NMDARs (GluN2A-NMDAR) in homocysteine-induced neurotoxicity (Poddar et al., 2017a; Poddar and Paul, 2009; Poddar and Paul, 2013). These findings further show that homocysteine-induced neurotoxicity involves sustained increase in extracellular-regulated kinase mitogen activated protein kinase (ERK, MAPK) phosphorylation, which involves a rapid initial increase followed by a delayed larger increase. This later increase in ERK MAPK phosphorylation is predominantly responsible for homocysteine-dependent neuronal cell death (Poddar and Paul, 2013). In addition to our findings, a more recent study performed in neuronal cultures indicates that homocysteine-induced increase in native NMDAR current preferentially involves GluN2A-NMDAR stimulation (Sibarov et al., 2016). This raises the possibility that homocysteine-induced intracellular signaling mechanisms act in concert with glutamate-mediated excitotoxic pathways to influence the pathology of stroke under hyperhomocysteinemic conditions.

A significant goal of the current study is to unravel whether hyperhomocysteinemia is a critical determinant of the severity of ischemic brain damage. To address this issue, we evaluated the pathophysiology and behavioral outcome of stroke in an animal model of hyperhomocysteinemia. Using non-invasive magnetic resonance imaging (MRI) approach and a battery of behavioral tests, we show that hyperhomocysteinemia exacerbates ischemic brain damage resulting in severe functional deficits. Pharmacological inhibition of GluN2A-NMDAR significantly reduces the extent of brain damage and functional deficits in the hyperhomocysteinemic rats, suggesting that exacerbation of ischemic brain injury under hyperhomocysteinemic conditions is mediated through GluN2A-NMDAR signaling. Consistent with this interpretation, hyperhomocysteinemia fails to exacerbate ischemic brain injury in GluN2A-knockout mice (GluN2A-KO), confirming the role of GluN2A-NMDARs in promoting ischemic brain injury under hyperhomocysteinemic conditions. The role of GluN2A-NMDAR signaling in exacerbation of ischemic brain injury under hyperhomocysteinemic condition strongly suggests that a single therapeutic approach targeting the glutamate/excitotoxic pathway may not be universally applicable to all ischemic stroke patients.

MATERIALS AND METHODS

Materials and reagents: L-homocysteine thiolactone hydrochloride, cytosine D-arabinofuranoside, glycine and Hoechst 33342 were obtained from Sigma-Aldrich (St. Louis, MO, USA). Selective pharmacological inhibitors were: Ro 256981 was obtained from Tocris, (Bristol, UK) and NVP-AAM077 (*[(R)-[(S)-1-(4-bromo-phenyl)-ethylamino]-(2,3-dioxo-1,2,3,4-tetrahydro-quinoxalin-5-yl)-methyl]phosphonic acid*) was a gift from Dr. Yves P Auberson, Novartis, (Basel, Switzerland). Anti-phospho ERK 1/2 (Thr202/Tyr204) monoclonal antibody

(pERK) and the anti-rabbit and anti-mouse horse-radish-peroxidase conjugated secondary antibodies were obtained from Cell Signaling Technology (Beverly, MA). Anti-ERK2 polyclonal antibody (ERK) was obtained from Santa Cruz Biotechnology (Dallas, TX). Bicinchoninic acid (BCA) protein estimation kit and West Pico supersignal chemiluminescence reagents for immunoblotting were obtained from Pierce (Rockland, IL). All reagents required for tissue culture studies were obtained from Life Technologies (Carlsbad, CA). Male Wistar rats were purchased from Envigo (Placentia, CA, USA). Rats were maintained in a 12-h light/dark vivarium (light off at 18.00 h) and with access to food and water ad libitum. Female time pregnant Sprague-Dawley rats were purchased from Envigo (Livermore, CA, USA) for establishing rat primary neuron cultures. GluN2A-NMDAR knockout mice (GluN2A-KO) was generated as previously described (Sakimura et al., 1995). They were obtained from Dr. Andrew Holmes, NIH/NIAAA, (Rockville, MD) and bred in the animal facility of University of New Mexico. Time pregnant female wild type (WT) and GluN2A-KO mice were generated at the animal facility of University of New Mexico for establishing mice neuronal cultures. All experiments were performed in accordance with protocols approved by the Institutional Animal Care Committee of University of New Mexico and were in compliance with the ARRIVE guidelines.

Development of hyperhomocysteinemic rat and mouse models: L-homocysteine (200 mM) was freshly prepared by alkali hydrolysis of L-homocysteine thiolactone hydrochloride followed by neutralization, and maintained in 0.02mM of *N*-Tris(hydroxymethyl)methyl-2-aminoethanesulfonic acid buffer pH 7.4 as described earlier (Poddar et al., 2001). Osmotic pumps (Alzet; 2ML1, flow rate 10 μ /hr) containing either 2 ml of freshly prepared 200 mM L-

homocysteine (for hyperhomocysteinemia) or normal saline (for control) were surgically implanted subcutaneously on the back and posterior to the scapulae of male Wistar rats under anesthesia (2% isoflurane in medical grade oxygen). The incision was closed after implantation and the rats were allowed to recover in their cage. For both WT and GluN2A-KO mice, osmotic pumps (Alzet; 2001, flow rate 1 μ l/hr) containing either 200 μ l of freshly prepared 200 mM L-homocysteine (for hyperhomocysteinemia) or normal saline (for control) were implanted similarly.

Measurement of total plasma homocysteine in rats and mice: Blood was obtained from rats (retro-orbital) and mice (cardiac puncture) under anesthesia with 2% isoflurane in medical grade oxygen, before installation of osmotic pumps (0 day) and at various time points after installation of osmotic pumps (rats: 3, 5 and 7 day; mice: 3 and 5 day). Blood was collected in standardized Vacutainer venous blood collection EDTA-tubes and centrifuged at 3,500 rpm for 15 min. The plasma obtained was analyzed for total plasma homocysteine levels using high performance liquid chromatography with post-column fluorescence detection as described earlier (Gilfix et al., 1997; Jacobsen et al., 1994; Miller et al., 2013).

Induction of transient focal cerebral ischemia: Middle cerebral artery occlusion (MCAO) was performed on both male rats and mice. For rat studies, control and hyperhomocysteinemic male Wistar rats (8-9 weeks, 290-295 g) were subjected to MCAO under anesthesia (2% isoflurane in medical grade oxygen), using the intraluminal method as described in our previous studies (Candelario-Jalil et al., 2004; Deb et al., 2013; Poddar et al., 2017b). Briefly, the right common carotid artery (CCA) was exposed through an incision made in the

ventral midline neck region. To prevent improper insertion of the occluding filament, both the external carotid artery and pterygopalatine branch of the internal carotid artery were clipped. A silicon-rubber-coated monofilament (403756, Doccol) was inserted into the internal carotid artery through an incision made in the CCA, 2 mm proximal from the bifurcation of the CCA, and advanced 18-19 mm from the bifurcation, to occlude the origin of the anterior cerebral, middle cerebral, and posterior communicating arteries. The incision was closed and the rats were allowed to recover from anesthesia. A quick assessment of neurological deficit was done immediately prior to reperfusion and only those animals that had more than 50% of contralateral forelimb flexion and walked in circles to the contralateral side were considered for the study (Longa et al., 1989). Following 60 min of occlusion, the rats were anesthetized and the filament was gently retracted to allow reperfusion. The incision was closed and the rats were allowed to recover from anesthesia. A subset of control and hyperhomocysteinemic rats received a single intravenous injection of GluN2A-NMDAR selective inhibitor NVP-AAM077 (1.2 mg/kg body weight) through the femoral vein, and another subset received a single intraperitoneal injection of GluN2B-NMDAR inhibitor Ro 256981 (6 mg/kg body weight) (Chaperon et al., 2003; Fox et al., 2006). Both NVP-AAM077 and Ro 256981 were administered at the onset of ischemic insult. The rats were then subjected to MRI on days 1, 3, and 14 post-MCAO and a series of behavioral tests was performed between Day 7-9, post-MCAO.

For biochemical studies control and hyperhomocysteinemic rats were subjected to sham surgery or MCAO for 60 min followed by reperfusion for 0, 3, 6, 12 or 24h. A sub-group of hyperhomocysteinemic rats were injected with NVP-AAM077 (1.2 mg/kg body weight) through the femoral vein at the onset of MCAO and sacrificed after 3h reperfusion. Rats were decapitated

at each of the above specified time points and the cortex from the ipsilateral hemisphere dissected on ice, briefly sonicated in Laemmli sample buffer, boiled at 100°C for 10 min, and processed for immunoblotting analyses (Deb et al., 2013).

For studies using WT and GluN2A KO mice (12-14 weeks, 26.5 – 27.5 g), MCAO was performed by the intraluminal method as described above. A silicon-rubber-coated monofilament (602234, Doccol) was advanced from an incision in the CCA through the internal carotid artery to a length of 10-11 mm from the bifurcation, occluding the middle cerebral artery. After 30 min of MCAO, the filament was removed to allow reperfusion, and the incision was closed. The mice were then subjected to MRI 24h after the ischemic insult.

Quantitation of infarct size and structural integrity by MRI: Multimodal MRI of rat brain that includes relaxation time imaging and diffusion imaging was performed at 1, 3 and 14 days after MCAO and reperfusion. The rats were placed in a dedicated holder, and positioned in the isocenter of a 4.7-Tesla MRI scanner (Bruker Biospin) that is equipped with a 40-cm bore and a gradient of 660 mT/m at rise time within 120 μ sec. To obtain good signal-to-noise ratio, a small-bore linear RF coil (inner diameter=72 mm) was used for signal excitation, and a single tuned surface coil (RAPID Biomedical, Rimpf, Germany) was used for signal detection (Poddar et al., 2017b; Sood et al., 2009; Taheri and Sood, 2007; Yang et al., 2013). For mice, the MRI was performed only at day 1. The mice were placed in its dedicated holder of inner diameter 72mm in the 4.7-Tesla MRI scanner with a 40-cm bore size and a gradient rise time / maximum speed of 9000 T/m/s. During MRI, the rats and mice were kept anesthetized with 2% isoflurane in medical grade oxygen. Respiration and heart rate were monitored continuously and body temperature was maintained at $37.0 \pm 0.5^\circ\text{C}$.

For rats, T2-weighted images were acquired with a rapid acquisition with relaxation enhancement (RARE) sequence of Repetition Time (TR)/Echo Time (TE)= 5,000 ms/56 ms, Field of View (FOV)= 4 cm × 4 cm, slice thickness = 1 mm, inter-slice distance = 1.1 mm, number of slices = 12, matrix = 256 × 256 and number of average = 3. For mice, T2 weighted images were acquired with a RARE sequence of Repetition Time / Echo Time = 5,000 ms/56 ms, Field of View = 4 cm × 4 cm, slice thickness = 1 mm, number of slices = 12, matrix = 256 × 256 and number of average = 3. The infarcted area was determined from T2 maps derived from the T2-weighted images by comparing regions of hyperintensity (infarcted or damaged area) and hypointensity (noninfarcted or undamaged area). An observer blinded to the experimental conditions evaluated the volume of ischemic brain damage from the T2 maps. For each slice, regions of hypointensity were highlighted on the ipsilateral side and the area measured. The total area on the contralateral side was also determined. The areas of hypointensity for the ipsilateral side and contralateral side were obtained by adding all slices together and the respective volumes were calculated by multiplying each sum by 1 (thickness of each section). The percentage of infarction volume was calculated as follows: [(volume of contralateral side – noninfarcted volume of the lesioned side)/volume of contralateral side] × 100 (Swanson et al., 1990).

Multi-slice, multi-shot, diffusion-weighted echo-planar imaging (Repetition Time / Echo Time = 3,800 ms/38 ms; b-values = 600 and 1,900 s/mm² in 30 directions; Field of View = 4 cm × 4 cm, slice thickness = 1 mm, matrix = 256 × 256) was performed to assess tissue architecture. Quantitative apparent diffusion coefficient (ADC) maps were calculated on a voxel-wise basis, with a linear least squares fit on the logarithm of the signal intensity versus the b-value for each diffusion direction. Based on the ADC maps, fractional anisotropy (FA) maps were generated using ParaVision 5.1 (Bruker Biospin MRI, Bellerica, MA, USA). Both the ADC

and FA values were computed for each slice and averaged over all the slices for the tissue. For MRI study, thirteen rats were subjected to MCAO in the control group, out of which one died within 24h. MRI scans were too noisy for one rat on day 1, one rat on day 3 and two rats on day 14. In the hyperhomocysteinemic group, MCAO was performed on twenty-six rats, out of which eleven died within 24 h. MRI scan was too noisy for one rat on day 14. These animals were therefore excluded from the MRI study on those days. In addition, ADC and FA values were not computed for one NVP-AAM077 treated hyperhomocysteinemic rat, as the processed maps were too noisy.

Behavioral Studies: All rats were subjected to a battery of behavioral tests on day 7 (CatWalk), day 8 (cylinder and rotarod tests) and day 9 (adhesive test) after MCAO to evaluate normal gait, motor coordination and sensory motor functions. Habituation and training (3 days) was performed for one week before MCAO. The first two trainings days were before osmotic pump implantation and the third training day was after pump implantation. An experienced observer blinded to the experimental conditions evaluated all behavioral parameters.

Catwalk: An automated quantitative gait analysis system (Catwalk XT 10.5, Noldus) was used to assess deficits in normal gait in the control, hyperhomocysteinemic and NVP-AAM077 treated hyperhomocysteinemic rats as described earlier (Parkkinen et al., 2013; Poddar et al., 2017b; Wang et al., 2008). Briefly, rats were trained to walk on a glass platform or walkway (1.3 m long and 90 mm wide) with a fluorescent light reflected internally in the glass floor as the rats cross the walkway, scattering at points where the paws touch the glass. A camera was positioned 56 cm below the walkway with intensity threshold set to 0.15, camera gain set to 17 and the

maximum allowed speed variation set to 60%. Pixels below the light intensity of 16 units on a 0 - 255 arbitrary scale were filtered out. A trial was regarded as successful if the animal did not have a maximum speed variation greater than 60% or did not stop on the runway. If an animal failed to complete a trial within 10 sec, walked backwards, or reared during the run, an additional re-run was performed. The camera recorded three such complete or successful runs across the walkway and the average of the three runs is reported. An experienced observer, blinded to the experimental group, labeled each paw on the recorded video and paw-related parameters were analyzed. The steps were automatically labeled as right fore paw (RF), right hind paw (RH), left fore paw (LF), and left hind paw (LH), where the right represents the non-impaired side and the left represents the impaired or affected side. Faulty labels caused by tail, whiskers, or genitalia were corrected. Automated analysis of wide range of parameters was performed: (A) The maximal contact area (expressed in mm^2), which is the paw area contacted at the moment of maximal paw-floor contact during stance was measured; (B) The print area (expressed in mm^2), which is the total floor area contacted by the paw during the stance phase was measured; (C) The print position (expressed in cm), which is the space relationship or distance between the former fore paw position to the consecutive hind paw position of the same side during one crossing of the walkway was evaluated. One control rat and one hyperhomocysteinemic rat were excluded from the study as they paused repeatedly during the run.

Cylinder test: Control, hyperhomocysteinemic and NVP-AAM077 treated hyperhomocysteinemic rats were subjected to cylinder test to assess the post-stroke asymmetry in fore-limb use (Balkaya et al., 2013; Poddar et al., 2017b). The rats were placed individually inside a transparent plexiglass cylinder (diameter 20 cm, height 45 cm). A vertical exploration

movement with either the left or right forelimb along the wall was scored as contact of each paw with the glass wall for a total period of 2 min. Simultaneous contact by both paws was scored separately. Two trials (10 min rest between trials) were recorded and the percentage use of the affected fore limb was calculated (Liu et al., 2013; Schaar et al., 2010). Six control rats and one hyperhomocysteinemic rat were excluded from the study, as they did not participate in the vertical exploration of the cylinder.

Accelerated Rotarod test: Control, hyperhomocysteinemic and NVP-AAM077 treated hyperhomocysteinemic rats were subjected to the accelerated Rotarod test to evaluate impairment of motor co-ordination and balance following stroke (Bouet et al., 2007; Dunham and Miya, 1957; Poddar et al., 2017b; Schaar et al., 2010). Rats were placed on a rotating cylindrical rod accelerating from 0 to 50 rpm for a period of 180 sec, and their latency to fall was recorded. The mean of four runs (10 min rest between trials) was used for statistical analysis. One hyperhomocysteinemic rat was excluded from the study as the rat jumped off the rod repeatedly.

Adhesive removal test: Sensorimotor deficits following stroke was assessed by performing the adhesive removal test in control, hyperhomocysteinemic and NVP-AAM077 treated hyperhomocysteinemic rats. A small adhesive patch (7 mm ×3 mm) was applied to the contralateral forepaw of each rat with equal pressure and the time taken to notice the presence of the patch (time to contact) and to remove it (time to remove) was recorded (Bouet et al., 2009; Poddar et al., 2017b). The time taken to notice the patch was recorded from the moment of placing the patch until the paw was shaken or touched by mouth. The time taken to remove the

patch was recorded from the moment the mouth touched the paw to the time the patch was removed. The trial ended after the adhesive patch was removed or a maximum latency of 3 min. The mean of three trials (10 min rest between tests) was used for statistical analysis.

Cresyl violet staining: On day 14 following MCAO, control, hyperhomocysteinemic and NVP-AAM077 treated hyperhomocysteinemic rats were anesthetized with isoflurane and perfused intracardially with 4% paraformaldehyde in 0.01M phosphate buffered saline pH 7.2 (PBS). Brains were removed, cryoprotected in 30% sucrose in PBS and then frozen in Optimal Cutting Temperature compound (OCT) kept in dry ice. Cresyl Violet Acetate staining was performed on 12 μ m cryosections. The fat was removed from the sections by immersing them in ethanol followed by chloroform. The sections were then re-hydrated by sequential exposure to decreasing concentrations of ethanol (100%, 95%, 70% and 0%) followed by staining with Cresyl Violet Acetate solution (5% Cresyl Violet acetate in glacial acetic acid-sodium acetate buffer, pH 3.7) for 8 min. The sections were differentiated in 0.1% glacial acetic acid in 70% ethanol for 30 sec followed by sequential dehydration in 95% and 100% ethanol and clearing with xylene. Finally, the sections were mounted with Cytoseal (DPX) and Multi Area Time Lapse images were obtained for the whole section using an Olympus microscope (10x objective).

Primary Neuron culture preparation and stimulation: Embryos obtained from time pregnant (1) Sprague Dawley female rats (16-17 day gestation), (2) WT mice and (3) GluN2A-KO mice (15-16 day gestation) were used to establish primary cortical neuronal cultures as described earlier (Poddar et al., 2017a; Poddar and Paul, 2009; Poddar and Paul, 2013). The neuron cultures were maintained in culture for 12-14 days and then treated with freshly prepared

L-homocysteine (50 μ M) in Hank's balanced salt solution containing 50 μ M of glycine (Lipton et al., 1997; Poddar et al., 2017a; Poddar and Paul, 2009; Poddar and Paul, 2013) for the specified time periods. In some of the neuron cultures obtained from rat embryos pharmacological inhibitors (NVP-AAM007, 30 nM; or Ro 25-6981 1 μ M) were added 10 min before exposure to homocysteine. At the specified time points cells were harvested and cell lysates were processed for immunoblotting studies.

Oxygen glucose deprivation (OGD) and Hoechst DNA staining: For OGD challenge, neurons were placed in an anaerobic chamber (Coy Laboratories; 95:5% of N₂:CO₂ gas mixture and maintained at 37⁰C) and incubated in balanced salt solution lacking glucose (116 mM NaCl, 5.4 mM KCl, 1 mM NaH₂PO₄, 1.8 mM CaCl₂, 26.2 mM NaHCO₃, 5 mM HEPES, 0.01 mM glycine, pH 7.4) as described earlier (Deb et al., 2013). Some cultures were exposed to L-homocysteine (50 μ M) during the OGD insult in the absence or presence of NVP-AAM077 (30 nM; 3h). At specified time periods (1, 2, and 3h) during OGD cells were removed from the chamber and lysed for immunoblot analysis. In some experiments after a 2h insult (OGD alone or OGD + L-homocysteine), the OGD medium was replaced with the original culture medium and then incubated at 37⁰C for an additional 22h in a humidified atmosphere (95:5% of air/CO₂ mixture). Cells were then subjected to staining with Hoechst 33342 dye for 15 min, washed extensively with PBS, and analyzed using fluorescent microscopy to assess nuclear damage. Imaging was performed with a Zeiss Axiovert 200M fluorescence microscope with attached AxioCam CCD camera using 20 \times objective lens (Carl Zeiss, Thornwood, NY, USA). To quantitatively assess the percentage of pyknotic nuclei, a total of 1000 cells were counted for each set of experiments (Poddar and Paul, 2009; Poddar and Paul, 2013).

Immunoblotting: Equal protein from total cell lysates obtained from rat and mice neuronal cultures as well as from brain lysates were resolved by SDS-PAGE (7.5%), and subjected to immunoblotting procedure as described earlier (Deb et al., 2013; Poddar and Paul, 2009). Blots were analyzed with anti-pERK and anti-ERK antibodies according to manufacturers recommendation. Signals from immune complexes in the blots were developed using West Pico supersignal chemiluminescence reagents and then captured on X-ray films. Densitometric analysis of the images was performed using Image J software.

Experimental design and statistical analysis: Data involving multiple groups were analyzed using one-way or two-way analysis of variance (ANOVA) as indicated and where assessment was performed across multiple days, the data was analyzed using repeated measure ANOVA (SPSS 24.0 software). Post-hoc analysis was done by Bonferroni's or Newman-Keuls multiple comparison tests. Vehicle vs. hyperhomocysteinemic groups or hyperhomocysteinemic vs. NVP- AAM077 treated hyperhomocysteinemic groups were considered as between group factor and days post-stroke as repeated factor. Analysis of two-group comparison was done using the Student's t-test. Data in the text and figures are expressed as means \pm SEM and differences were considered statistically significant when $p < 0.05$. Pearson's r was used for effect size calculation for all t-test data (Mukaka, 2012). Power calculations were run using G* power (3.1.9.2). For the one-way ANOVA, using an effect size of 0.60, an alpha of .05 and $n = 13$ per treatment group produced 83% power. A sensitivity test using a one-way ANOVA with $n = 13$ and a power of 80% at an alpha level of .05 indicates that we have sufficient sample size to detect an effect size of 0.57 and for the repeated measure ANOVA we can detect an effect size of

0.256 with 80% power. Achieved power for the repeated measures ANOVA (2 between and 3 repeated measures) with an effect size of 0.7, an alpha of .05, and $n = 12$ per treatment group produced a power of 99%. For the lowest significant t-test the effect size was 0.507, the calculated power was determined to be 76% with the given sample sizes $n = 10$ for vehicle and $n = 12$ for hyperhomocysteinemia. Thus, there is sufficient power in the data set to justify the conclusions.

RESULTS

Hyperhomocysteinemia exacerbates ischemic brain injury in rats

In initial studies, blood samples were obtained from control and hyperhomocysteinemic rats at different time intervals as outlined in Figure 1A, for analysis of total plasma homocysteine. Figure 1B shows that total plasma homocysteine level prior to pump implantation is $8.8 \pm 0.76 \mu\text{M}$. This basal level does not change significantly in the control rats with the installation of saline containing pumps. However, installation of L-homocysteine containing pumps increases total plasma homocysteine level to $23.2 \pm 0.52 \mu\text{M}$ ($p < 0.0001$; $r = 0.969$) within 3 days that remains sustained for the time period of the study (day 5: $23.57 \pm 0.57 \mu\text{M}$; $p < 0.0001$; $r = 0.9663$, day 7: 20.52 ± 0.88 ; $p < 0.0001$, $r = 0.954$).

In subsequent experiments control and hyperhomocysteinemic rats were subjected to either sham surgery or MCAO (60 min), 4 days after pump implantation, followed by reperfusion. Infarct size and functional outcome were assessed as outlined in Figure 2A. Our findings show that ischemic insult under hyperhomocysteinemic (HHcy) condition increases the mortality rate substantially when compared with the control group (Fig. 2B; control: 7.69% vs.

HHcy: 42.3%). The surviving animals were subjected to MRI 24h after MCAO to assess the extent of ischemic brain injury. The representative T2 maps show regions of increased T2 signal intensity in the stroked hemisphere of both control and hyperhomocysteinemic rats indicating ischemic lesion (Fig. 2C). The spatial distribution of ischemic lesion in hyperhomocysteinemic rats extends to both anterior and posterior cortex, regions that are unaffected in the control rats. Figure 2C further show that in the absence of an ischemic insult hyperhomocysteinemia by itself does not cause any brain lesion (compare control sham vs. hyperhomocysteinemic sham). Quantitative analysis of lesion volume in control and hyperhomocysteinemic rats subjected to MCAO (Fig. 2D) shows a significant increase in infarct size under hyperhomocysteinemic condition (control: $18.36 \pm 2.85\%$ vs. HHcy: $37.41 \pm 2.33\%$; $p < 0.0001$, $r = 0.716$).

Long-term progression of ischemic damage in hyperhomocysteinemic rats

Longitudinal evaluation of ischemic lesion volume in control and hyperhomocysteinemic rats up to 14 days post-MCAO show significant group effect [$F_{(1, 22)} = 26.39$, $p < 0.0001$] and day effect [$F_{(2, 44)} = 17.702$, $p < 0.0001$] between the two groups. However, treatment by day interaction is not significant. The representative T2 maps and quantitative measurement of lesion volume from the T2 maps (Fig. 3A) show that the infarct size remains significantly higher in the hyperhomocysteinemic rats at both day 3 (control: $21.94 \pm 2.74\%$ vs. HHcy: $38.63 \pm 2.75\%$) and day 14 (control: $13.81 \pm 2.77\%$ vs. HHcy: $27.16 \pm 2.18\%$) after MCAO. The representative ADC and FA maps and the quantitative analysis of ADC and FA values, evaluated at 14-day post-MCAO, show significant increase in the ADC value (control: $1.01 \times 10^3 \pm 0.01 \times 10^3 \text{ mm}^2/\text{sec}$ vs. HHcy: $1.41 \times 10^3 \pm 0.06 \times 10^3 \text{ mm}^2/\text{sec}$; $p = 0.002$; $r = 0.587$) with concomitant decrease in FA value (control: 0.3 ± 0.02 vs. HHcy: 0.25 ± 0.01 ; $p = 0.049$; $r = 0.405$) in the

hyperhomocysteinemic rats (Fig. 3B and C). This pattern of increased mean diffusion with decreased directional diffusion as observed from the ADC and FA data respectively suggests that an ischemic insult under hyperhomocysteinemic condition accelerates tissue breakdown resulting in greater loss of structural integrity and orientation of the brain tissue in the infarcted area. For histopathological confirmation of the ischemic lesion observed using MRI at 14-day post-MCAO brain sections from both control and hyperhomocysteinemic rats were processed for cresyl violet staining. The representative photomicrographs presented in Figure 3D shows that the characteristic pattern of lesion observed by cresyl violet staining is comparable to the ischemic lesion detectable in T2 maps (Fig. 3A).

Exacerbation of ischemic brain damage in hyperhomocysteinemic rats is dependent on GluN2A-NMDAR

To delineate the role of GluN2A- and GluN2B-NMDAR subunits in exacerbation of ischemic brain injury under hyperhomocysteinemic condition we evaluated the effect of NVP-AAM077, which preferentially inhibits GluN2A-NMDARs (Auberson et al., 2002; Chaperon et al., 2003), and Ro 25-6981, the selective inhibitor of GluN2B-NMDARs (Fischer et al., 1997; Mutel et al., 1998). Both control and hyperhomocysteinemic rats were subjected to 60min MCAO followed by reperfusion (24h) and NVP-AAM077 or Ro 256981 was injected at the onset of the ischemic insult. The representative T2 maps from control and hyperhomocysteinemic rats treated with NVP-AAM077 (Fig. 4A) and quantitative analysis of mean lesion volume (Fig. 4B, C) by two-way ANOVA followed by t-test reveals a significant effect of HHcy [$F(1, 45) = 13.5, p = 0.001$] and NVP-AAM077 [$F(1,45) = 15.4, p = 0.001$] and an interaction between NVP-AAM077 and HHcy [$F(1,45) 9.01, p = 0.004$]. The interaction

demonstrates that inhibition of GluN2A-NMDARs with NVP-AAM077 fails to reduce the infarct size in the control rats (Fig. 4B; control: $18.65 \pm 2.89\%$ vs. control + NVP: $16.07 \pm 2.8\%$; $p = 0.530$; $r = 0.137$), which has also been observed in an earlier study (Liu et al., 2007). In contrast, inhibition of GluN2A-NMDARs in hyperhomocysteinemic rats reduces mortality (HHcy: 42.3% vs. HHcy + NVP-AAM077: 15.4%) as well as ischemic infarct size (Fig. 4C; HHcy: $37.41 \pm 2.33\%$ vs. HHcy + NVP AAM077: $17.98 \pm 3.24\%$; $p < 0.0001$; $r = 0.714$) to a level that is comparable with the infarct size observed in the control rats ($p = 0.8744$; $r = 0.035$). On the other hand, analysis of mean lesion volume following inhibition of GluN2B-NMDARs with Ro 256981 (Fig. 4A, D, E) reveals a significant effect of HHcy [$F(1,39) = 62.3$, $p = 0.001$] and an effect of Ro 256981 [$F(1,39) = 8.5$, $p = 0.006$]. The findings show that inhibition of GluN2B-NMDARs significantly reduces infarct size in the control rats (Fig. 4D; control: $18.65 \pm 2.89\%$ vs. control + Ro 256981: $7.46 \pm 1.24\%$; $p = 0.002$; $r = 0.618$) and is consistent with earlier findings (Gogas, 2006; Liu et al., 2007; Parsons et al., 1998). Inhibition of GluN2B-NMDARs in hyperhomocysteinemic rats also results in a small but non-significant decrease in infarct size (Fig. 4E; HHcy: $37.41 \pm 2.33\%$ vs. HHcy + Ro 256981: $32.48 \pm 4.32\%$; $p = 0.286$; $r = 0.237$). The inability of the GluN2A-NMDAR inhibitor to reduce ischemic lesion volume in the control rats suggest that in the absence of any underlying comorbidity, the progression of ischemic brain damage is primarily mediated through GluN2B-NMDAR signaling. However, in the presence of the comorbid condition of hyperhomocysteinemia GluN2A-NMDAR activation plays an additional role in the exacerbation of the ischemic brain damage.

In subsequent studies, ischemic lesion volume in hyperhomocysteinemic rats treated with or without NVP-AAM077 was evaluated up to 14 days post-MCAO to assess the late

manifestation of brain injury following treatment. Longitudinal evaluation of the infarct size show significant group difference [$F_{(1, 23)} = 26.891$, $p < 0.0001$] and day effect [$F_{(2, 46)} = 14.891$, $p < 0.0001$] between NVP-AAM077 treated and untreated hyperhomocysteinemic rats. However, treatment by day interaction is not significant. The representative T2 maps and *post hoc* analysis of the lesion volume (Fig. 5A) show that NVP-AAM077 treated group has significantly smaller lesion size at both day 3 (HHcy: $38.63 \pm 2.75\%$ vs. HHcy + NVP-AAM077: $19.61 \pm 4.48\%$) and day 14 (HHcy: $27.16 \pm 2.18\%$ vs. HHcy + NVP-AAM077: $10.76 \pm 2.40\%$) after MCAO. Evaluation of the structural integrity of the brain tissue in the infarcted area at day 14 show a significant decrease in ADC value (HHcy: $1.41 \times 10^3 \pm 0.06 \times 10^3 \text{ mm}^2/\text{sec}$ vs. HHcy + NVP-AAM077: $1.16 \times 10^3 \pm 0.05 \times 10^3 \text{ mm}^2/\text{sec}$; $p = 0.003$; $r = 0.574$) and concomitant increase in FA value (HHcy: 0.25 ± 0.01 vs. HHcy + NVP-AAM077: 0.32 ± 0.01 ; $p = 0.002$; $r = 0.599$) following treatment with NVP-AAM077, reflecting reduced tissue breakdown and less accumulation of extracellular water in the residual stroke cavity (Fig. 5B, C). These findings indicate that the effect of early treatment with NVP-AAM077 is not transient.

Inhibition of GluN2A-NMDARs reduces behavioral deficits following ischemia in hyperhomocysteinemic rats

We next investigated the effect of ischemic brain injury on post-stroke behavioral impairment in the control, hyperhomocysteinemic and NVP-AAM077 treated hyperhomocysteinemic rats. Assessment of gait parameters using CatWalk, one week after stroke reveals significant differences between the treatment groups for maximum contact area [$F_{(2, 33)} = 4.956$, $p = 0.0131$], print area [$F_{(2, 33)} = 5.776$, $p = 0.007$] and print position [$F_{(2, 33)} = 6.129$, $p = 0.005$] by one-way ANOVA. Post hoc analyses further show that the maximum

contact area of the affected forepaw in hyperhomocysteinemic rats is significantly reduced when compared to control rats (Fig. 6A; control: 1.09 ± 0.056 vs. HHcy: 0.8 ± 0.082 ; $p < 0.05$). In contrast, treatment with NVP-AAM077 significantly increases the maximum contact area of the affected paw when compared to the untreated hyperhomocysteinemic group (Fig. 6A; HHcy: 0.8 ± 0.082 vs. HHcy + NVP-AAM077: 1.11 ± 0.092 ; $p < 0.05$). Similarly, the print area is significantly lesser for hyperhomocysteinemic rats when compared with the control rats (Fig. 6B; control: 1.42 ± 0.063 vs. HHcy: 1.06 ± 0.097 ; $p < 0.05$). However, a significant improvement in print area is observed following treatment with NVP-AAM077 (Fig. 6B; HHcy: 1.06 ± 0.097 vs. HHcy + NVP-AAM077: 1.41 ± 0.092 ; $p < 0.05$). In addition, the print position of the affected side is significantly less in the hyperhomocysteinemic rats when compared to the control rats (Fig. 6C; control: 1.4 ± 0.19 vs. HHcy: 0.72 ± 0.15 ; $p < 0.05$), which returns to control levels following treatment with NVP-AAM077 (Fig. 6C; HHcy: 0.72 ± 0.15 vs. HHcy + NVP-AAM077: 1.37 ± 0.097 ; $p < 0.05$).

Evaluation of the spontaneous usage of the affected forelimb using cylinder test show significant difference between the treatment groups [$F_{(2, 29)} = 22.98$, $p < 0.0001$]. Figure 6D shows that the usage of the affected forepaw in hyperhomocysteinemic rats is significantly less as compared to control rats (control: $43.73 \pm 1.61\%$ vs. HHcy: $24.24 \pm 2.37\%$; $p < 0.0001$), and treatment with NVP-AAM077 results in significant improvement in spontaneous usage of the affected forepaw in hyperhomocysteinemic rats (HHcy: $24.24 \pm 2.37\%$ vs. HHcy + NVP-AAM077: 40.51 ± 1.86 ; $p < 0.0001$).

Evaluation of motor coordination and balance using accelerated rotarod show significant difference between the treatment groups [$F_{(2, 34)} = 5.813$, $p = 0.006$]. Rotarod performance of each group show that hyperhomocysteinemic rats are significantly less efficient in maintaining balance on the rotarod as compared to the control rats (Fig. 6E; control: 118.5 ± 5.31 sec vs. HHcy: 96.99 ± 4.11 sec; $p < 0.05$), while treatment with NVP-AAM077 significantly enhances the performance of hyperhomocysteinemic rats (Fig. 6E; HHcy: 96.99 ± 4.11 sec vs. HHcy + NVP-AAM077: 112.51 ± 4.9 sec; $p < 0.05$).

Evaluation of sensory motor deficit using adhesive test show significant group differences for both the time to make contact [$F_{(2, 35)} = 26.42$, $p < 0.0001$] and the time to remove [$F_{(2, 35)} = 42.57$, $p < 0.0001$] the adhesive tape from the contralateral forepaw. Figure 6F and G shows that hyperhomocysteinemic rats take significantly longer time to contact (control: 30.61 ± 4.69 s vs. HHcy: 76.82 ± 5.45 s; $p < 0.0001$) and remove (control: 54.53 ± 6.51 s vs. HHcy: 127.86 ± 7.29 s; $p < 0.0001$) the tape when compared to the control rats. On the other hand, treatment of hyperhomocysteinemic rats with NVP-AAM077 significantly reduces both the time to contact (HHcy: 76.82 ± 5.45 s vs. HHcy + NVP-AAM077: 31.18 ± 5.68 s; $p < 0.0001$) and remove (HHcy: 127.86 ± 7.29 s vs. HHcy + NVP-AAM077: 44.24 ± 7.59 s; $p < 0.0001$) the tape, indicating an improvement in both sensory and motor skill.

Genetic deletion of GluN2A-NMDARs mitigates ischemic brain injury in hyperhomocysteinemic mice

We next examined whether deletion of endogenous GluN2A-NMDARs could attenuate the exacerbation of ischemic brain damage observed under hyperhomocysteinemic condition. In

initial studies osmotic pumps containing L-homocysteine were installed in both WT and GluN2A-KO mice and blood samples were collected on day 0 (before pump installation) and days 3 and 5 after pump implantation for analysis of plasma homocysteine level (outlined in figure 7A). Figure 7B shows that total plasma homocysteine in WT mice increases from $6.6 \pm 0.73 \mu\text{M}$ (day 0) to $18.97 \pm 1.68 \mu\text{M}$ on day 3 ($p < 0.01$) and remains elevated at $16.68 \pm 1.73 \mu\text{M}$ on day 5 ($p < 0.01$). In GluN2A-KO mice, the total plasma homocysteine level also increases from $5.72 \pm 0.33 \mu\text{M}$ (day 0) to $18.46 \pm 2.55 \mu\text{M}$ on day 3 ($p < 0.01$) that remain elevated at $15.92 \pm 2.09 \mu\text{M}$ on day 5 ($p < 0.01$). In subsequent studies, WT and GluN2A-KO mice implanted with saline pump (control) or homocysteine pump (hyperhomocysteinemic) were subjected to MCAO (30 min) 4 days after pump implantation. This was followed by reperfusion and assessment of infarct size by MRI 24h after MCAO. The mild ischemic insult in the WT and GluN2A-KO control mice did not result in any mortality within the time period of our study, whereas in hyperhomocysteinemic WT mice 28.5% mortality is observed in the same time period. Ischemic insult in the hyperhomocysteinemic GluN2A-KO mice also did not result in any mortality during this period. The representative T2 maps (Fig. 7C) and quantitative analysis of lesion volumes in the surviving mice (Fig. 7D) by two way ANOVA followed by t-test reveals a significant effect of genotype [$F(1,15)=12.2$, $p = 0.003$] and HHcy [$F(1,15) = 13.02$, $p = 0.003$], as well as an interaction between genotype and HHcy [$F(1,15)= 14.13$, $p = 0.002$]. The interaction shows that ischemic insult in both the WT control mice and GluN2A-KO control mice result in a small infarct size that is limited to the striatum (WT control: $13.52 \pm 3.13\%$ vs. GluN2A-KO control: $14.85 \pm 3.8\%$, $p = 0.82$; $r = 0.077$) and is consistent with earlier findings (Deb et al., 2013). However, ischemic insult in the hyperhomocysteinemic WT mice results in significant exacerbation of the ischemic brain damage that encompasses the striatum and the

cortex (WT control: $13.52 \pm 3.12\%$ vs. WT HHcy: $50.28 \pm 6.54\%$; $p = 0.0001$; $r = 0.864$). These findings are in agreement with our previous results in rats (Fig 2C and D), suggesting that regardless of species, hyperhomocysteinemic condition exacerbates ischemic brain injury. However, such exacerbation of ischemic brain injury is not observed in hyperhomocysteinemic GluN2A-KO mice (GluN2A-KO control: $14.85 \pm 3.8\%$ vs. GluN2A-KO HHcy: 14.1 ± 1.77 ; $p = 0.867$; $r = 0.088$), confirming a role of GluN2A-NMDARs in hyperhomocysteinemia-induced exacerbation of ischemic brain injury.

Mechanistic basis of GluN2A-NMDAR dependent exacerbation of ischemic brain injury under hyperhomocysteinemic condition.

To examine the role of GluN2A-NMDARs in homocysteine induced delayed ERK MAPK phosphorylation in initial studies cortical neuronal cultures were treated with L-homocysteine ($50 \mu\text{M}$, 4h) in the presence or absence of NVP-AAM077 or Ro 25-6981. Figure 8A shows significant increase in ERK MAPK phosphorylation 4h after homocysteine treatment, which is consistent with our earlier findings (Poddar and Paul, 2013). Incubation of neurons with NVP-AAM077 blocks homocysteine-induced ERK MAPK phosphorylation. In contrast, Ro 25-6981 has no effect on the homocysteine-mediated ERK MAPK phosphorylation. In subsequent studies neuron cultures obtained from WT and GluN2A-KO mice were exposed to L-homocysteine treatment ($50 \mu\text{M}$, 4h). Figure 8B shows that homocysteine treatment leads to significant increase in ERK MAPK phosphorylation in the neuronal cultures obtained from WT mice, while it remains unchanged in the neurons obtained from GluN2A-KO mice, when compared to the respective untreated controls. These findings confirm the role of GluN2A-NMDAR in homocysteine-induced delayed ERK MAPK phosphorylation that has been shown to be

responsible for homocysteine-induced neuronal cell death (Poddar and Paul, 2009; Poddar and Paul, 2013).

We next exposed neuronal cultures to OGD (1, 2 and 3h) to mimic ischemic injury, for assessment of ERK MAPK phosphorylation profile in the absence or presence of homocysteine. Immunoblot analysis shows that OGD insult alone leads to a rapid but transient increase in ERK MAPK phosphorylation by 1h (Fig. 8C). In contrast, OGD in the presence of homocysteine leads to sustained increase in ERK MAPK phosphorylation throughout the time course examined (Fig. 8C). To evaluate the role of GluN2A-NMDAR in the sustained ERK MAPK phosphorylation, neurons were exposed to OGD and L-homocysteine in the presence of NVP-AAM077 for 3h. Figure 8D shows that treatment with NVP-AAM077 inhibits ERK MAPK phosphorylation in neurons exposed to OGD in the presence of L-homocysteine. To further determine whether the sustained ERK MAPK phosphorylation observed following OGD in the presence of L-homocysteine is also associated with enhanced neuronal injury, neuronal cultures were subjected to OGD for 2 hr in the presence of homocysteine (50 μ M) and then maintained in re-oxygenated conditions for 22 hr. Quantitative analysis of the extent of cell death shows that OGD-induced cell death increases by 2-fold in the presence of homocysteine (Fig. 8E).

We next investigated whether a mild ischemic insult under hyperhomocysteinemic condition could lead to prolonged increase in ERK MAPK phosphorylation, similar to what we have observed in cultured neurons exposed to OGD in the presence of homocysteine (Fig. 9A). For these experiment both normal and hyperhomocysteinemic Wistar rats were subjected to MCAO for 60 min followed by reperfusion for specified time periods (0, 3, 6, 12h). Immunoblot analysis of tissue punches from the ipsilateral cortex show that, during the insult, (I60/0h RPF)

ERK MAPK phosphorylation increases significantly in the hyperhomocysteinemic rats when compared to control rats, and it remains sustained during reperfusion (Fig. 9A). We then determined whether administration of NVP-AAM077 could block the sustained phosphorylation of ERK MAPK in hyperhomocysteinemic rats at 3h of reperfusion. Figure 9B shows a significant reduction in ERK MAPK phosphorylation in hyperhomocysteinemic rats when treated with NVP-AAM077. The findings highlights the role of GluN2A-NMDAR in sustained ERK MAPK phosphorylation following ischemic insult under hyperhomocysteinemic condition.

DISCUSSION

The key finding of the current study is that mild hyperhomocysteinemia leads to exacerbation of brain damage and significant deficits in sensory motor function following a transient cerebral ischemia. Importantly, the study also show that pharmacological inhibition of GluN2A-NMDARs significantly reduces ischemic brain damage in hyperhomocysteinemic rats but does not alter ischemic lesion size in rats with normal homocysteine level, indicating that exacerbation of brain injury under hyperhomocysteinemic condition involves GluN2A-NMDAR activation. Consistent with this interpretation, studies in GluN2A-KO mice further show that in the absence of GluN2A-NMDARs, hyperhomocysteinemia fails to exacerbate ischemic brain damage, validating the role of GluN2A-NMDARs in hyperhomocysteinemia-induced brain injury during an ischemic insult. Biochemical studies further show that GluN2A-NMDAR mediated ERK MAPK activation is a critical mediator of neuronal injury in the presence of homocysteine that could act in concert with cytotoxic pathways activated following an ischemic insult to exacerbate ischemic brain damage under hyperhomocysteinemic condition. To the best of our knowledge the current study provides the first evidence that GluN2A-NMDARs, which

generally is thought to promote neuronal survival (Chen et al., 2008; Kim et al., 2005; Liu et al., 2007; Riccio and Ginty, 2002; Zhang et al., 2007), could also play an important role in neurodegeneration.

To understand the pathophysiology of elevated plasma homocysteine in humans, it is critically important to develop animal models of hyperhomocysteinemia where the pathophysiological outcome could be directly related to the elevated level of homocysteine. Several animal models are currently in use to study the pathophysiology of hyperhomocysteinemia that includes diets deficient in vitamin B12 and/or folate (Duan et al., 2002; Endres et al., 2005; Kruman et al., 2002); diet supplemented with high methionine, the precursor of homocysteine (Dayal et al., 2004; Morita et al., 2001; Ungvari et al., 1999; Zhang et al., 2010); a vitamin deficient diet combined with methionine supplementation (Dayal et al., 2004; Morita et al., 2001; Zhang et al., 2010); and genetic models where enzymes that are involved in homocysteine metabolism are targeted (Dayal and Lentz, 2008). These dietary and genetic manipulations are known to interfere with homocysteine metabolism leading to elevated plasma levels of homocysteine. Utilizing these animal models of hyperhomocysteinemia earlier studies evaluated the effect of elevated plasma homocysteine in vascular cell dysfunction, endothelial cell remodeling and BBB disruption (Dayal and Lentz, 2008; Devlin et al., 2004; Kalani et al., 2014; Kamath et al., 2006; Kruman et al., 2002). However, a major limitation of these models is that in addition to elevation of plasma homocysteine, there are alterations in other metabolic pathways and therefore the pathophysiological outcome observed in these models cannot be attributed to hyperhomocysteinemia alone (Dayal and Lentz, 2008; Endres et al., 2005). To overcome this problem, some studies have used an animal model of

hyperhomocysteinemia, generated by implanting osmotic pumps containing homocysteine to provide slow and continuous systemic infusion of homocysteine that could allow direct evaluation of the pathophysiology of hyperhomocysteinemia (Chen et al., 2002; Christie et al., 2005). Using this approach, we developed rodent models of mild hyperhomocysteinemia where total plasma homocysteine increases to $\sim 23 \mu\text{M}$ in rats and $\sim 19 \mu\text{M}$ in mice within 3 days of pump implantation. A comparison of the brain MRI images obtained from control and hyperhomocysteinemic rats further show that mild hyperhomocysteinemia by itself does not result in any vasogenic edema, typically caused by pathogenic increase in BBB permeability (Michinaga and Koyama, 2015). This finding suggests that such mild elevation of plasma homocysteine level does not exert any detrimental effect on the brain through adverse action on the vasculature and is consistent with an earlier observation, which showed that BBB function in rodents is not compromised at this level of plasma homocysteine (Kamath et al., 2006). Our findings also show that ischemic insult under such mild hyperhomocysteinemic condition leads to exacerbation of brain injury within 24h that remains elevated upto 3 days post-MCAO. Thereafter, the brain experiences a spontaneous recovery process resulting in partial reduction in the lesion size in both the control and hyperhomocysteinemic rats, which is consistent with earlier findings (Clark et al., 1993; Knight et al., 1991; Li et al., 2014; Li et al., 2004; Poddar et al., 2017b; Rewell et al., 2017; Takamatsu et al., 2002; Virley et al., 2000). However, the lesion size in the hyperhomocysteinemic rats remains significantly large on day 14 post-MCAO, when compared to the ischemic lesion size in the control rats. These findings suggest that disruption of the blood-brain barrier after an acute ischemic stroke under hyperhomocysteinemic conditions exposes brain cells to plasma levels of homocysteine resulting in increased brain injury. In addition, the increase in ADC value within the lesion area of hyperhomocysteinemic animals

reflects an increase in accumulation of extracellular water, tissue cavitation and gliosis (Schaefer et al., 2000; Shen et al., 2011; Sotak, 2002). The concomitant decrease in FA value within the lesion area of hyperhomocysteinemic animals reflects an elevated radial diffusivity and is indicative of loss of tissue structural integrity and orientation (Johansen-Berg and Behrens, 2014; Pitkonen et al., 2012; Sotak, 2002). Consistent with these findings, functional evaluation of normal gait, motor coordination and sensory motor function also shows significant deterioration under hyperhomocysteinemic condition. These differences in the stroke outcome between hyperhomocysteinemic and normal rats strongly suggest that additional deleterious pathways are activated under hyperhomocysteinemic conditions, following an ischemic insult.

Earlier studies have shown that excessive release of the neurotransmitter glutamate and over activation of the NMDA subclass of glutamatergic receptors plays a central role in ischemic brain injury. In the adult forebrain, where stroke most frequently occur, NMDARs are predominantly composed of heteromeric assemblies of GluN1/GluN2A, GluN1/GluN2B or GluN1/GluN2A/GluN2B subunits (Hardingham et al., 2002; Kim et al., 2005; Li et al., 2002; Liu et al., 2007; Zhang et al., 2007) and the subunit composition determines receptor function under physiological and pathological conditions. GluN2A-NMDARs have been shown to play a role in synaptic plasticity including long-term potentiation and spatial memory formation (Dingledine et al., 1999; Hardingham and Bading, 2003; Lynch and Guttman, 2002; Scimemi et al., 2004; Vicini et al., 1998). Furthermore, growth and survival-promoting signals have been shown to be derived primarily from GluN2A-NMDARs (Liu et al., 2007; Martel et al., 2012; Papadia et al., 2005; Terasaki et al., 2010). In contrast, long-term depression and death-promoting signal have been shown to be generally triggered by GluN2B-NMDARs (Chen et al., 2008; Dalton et al.,

2012; Foster et al., 2010; Fox et al., 2006; Liu et al., 2007; Soriano et al., 2008; Tu et al., 2010). Consistent with these findings, several *in vitro* and *in vivo* studies on excitotoxic and ischemic neuronal injury have demonstrated that selective inhibition of GluN2A-NMDAR either has no effect or exacerbate neuronal death (Chen et al., 2008; DeRidder et al., 2006; Liu et al., 2007; Morikawa et al., 1998), whereas selective GluN2B-NMDAR antagonists are highly neuroprotective (Chen et al., 2008; DeRidder et al., 2006; Lai et al., 2011; Liu et al., 2007; Schumann et al., 2008). In spite of this general consensus on the role of GluN2A-NMDARs in neuroprotection a few studies have indicated a causal role of GluN2A-NMDAR in excitotoxicity (Morikawa et al., 1998; Wang et al., 2003; Zhou et al., 2013). However, the interpretation of the results obtained from these studies also show that under severe pathological condition GluN2A-NMDARs does not have a measurable contribution and GluN2B-NMDARs plays a more dominant role in excitotoxicity (Martel et al., 2012; Morikawa et al., 1998; Zhou et al., 2013).

Our findings now provide strong evidence for a novel role of GluN2A-NMDAR in mediating the detrimental effects of homocysteine to accelerate stroke-induced brain damage under hyperhomocysteinemic condition. A comparison of the anatomical T2 maps, ADC and FA values acquired from hyperhomocysteinemic animals subjected to a mild ischemic insult and treated with or without NVP-AAM077, show a significant reduction in ischemic lesion size and improved structural integrity within the lesion area following treatment. Behavioral studies also show a significant improvement in normal gait and sensory motor function following treatment. It is important to note here that the dose of NVP-AAM077 used in our study is within the dose range used in multiple studies to preferentially inhibit GluN2A-NMDARs (Auberson et al., 2002; Dalton et al., 2012; Fox et al., 2006; Liu et al., 2004; Liu et al., 2007; Massey et al., 2004;

Tigaret et al., 2006). To further assess any potentially nonselective effect of NVP-AAM077 on GluN2B-NMDARs, in additional studies we compared the effect of blocking GluN2A-NMDAR or GluN2B-NMDAR on ischemic brain damage in the control rats. The efficacy of GluN2B-NMDAR antagonist Ro 25-6981, but not GluN2A-NMDAR inhibitor NVP-AAM077 in reducing ischemic brain damage in the control rats indicates that ischemic brain damage in the absence of hyperhomocysteinemia is primarily mediated through GluN2B-NMDARs. The findings also confirm the role of NVP-AAM077 in selectively blocking GluN2A-NMDARs in attenuating ischemic brain damage under hyperhomocysteinemic conditions. Further validation for a role of GluN2A-NMDAR in the exacerbation of ischemic brain injury under hyperhomocysteinemic condition comes from additional studies in GluN2A-KO mice. The findings show that in the absence of GluN2A-NMDARs, ischemic lesion volume does not increase with elevated levels of total plasma homocysteine, and is in agreement with the results obtained with the pharmacological blockade of GluN2A-NMDARs in rats.

The distinctly different contribution of GluN2A- and GluN2B-NMDARs in the progression of ischemic brain damage under hyperhomocysteinemic condition could not be attributed to differential signaling through synaptic and extrasynaptic NMDARs. This is because, in the absence of a clear definition of synaptic and extrasynaptic NMDARs it is difficult to estimate the proportion of GluN2A-NMDAR localized in these two regions. This difficulty is evident especially when one tries to reconcile data from microscopy, electrophysiology and pharmacological approaches (Papouin and Oliet, 2014). From the morphological point of view, receptors are often considered extrasynaptic if they are situated more than 100 nm away from the post-synaptic density (Hardingham and Bading, 2010; Petralia et al., 2010). From the

electrophysiological point of view, synaptic NMDARs are those that are recruited during afferent stimulation at low frequency or in response to spontaneous glutamate release. While extrasynaptic NMDARs correspond to receptors that are not activated during such conditions (Chen and Diamond, 2002; Clark and Cull-Candy, 2002; Harris and Pettit, 2007; Harris and Pettit, 2008; Lozovaya et al., 2004; Papouin and Oliet, 2014; Tovar and Westbrook, 1999). This electrophysiological definition of synaptic NMDARs may include receptors located not only at synapses but also at extrasynaptic locations that could contribute to low-frequency synaptic transmission (Papouin and Oliet, 2014). From a pharmacological perspective, it is also not clear whether synaptic and extrasynaptic NMDARs have distinct subunit composition. Several studies suggest that GluN2B-NMDARs are preferentially found at extrasynaptic locations, while others suggest that this localization is not specific and GluN2B-NMDARs can also be found at synaptic sites (Barria and Malinow, 2002; Gladding and Raymond, 2011; Harris and Pettit, 2007). As such the data obtained from this study does not delineate the localization of GluN2A-NMDAR between synaptic and extrasynaptic regions.

Another important finding of the current study is that the increase in neuronal cell death in the *in vitro* model of ischemia (OGD) in the presence of homocysteine, and exacerbation of ischemic brain injury under hyperhomocysteinemic condition are associated with sustained increase in ERK MAPK phosphorylation. Pharmacological inhibition of GluN2A-NMDAR attenuates such increase in ERK MAPK phosphorylation substantiating a role of GluN2A-NMDAR dependent ERK MAPK signaling in the increased neuronal injury (*in vitro*) and brain damage (*in vivo*) observed in the presence of homocysteine. Consistent with this interpretation, in an earlier study we have demonstrated that treatment of neurons with homocysteine alone

could lead to such sustained ERK MAPK phosphorylation, and pharmacological inhibition of ERK MAPK could attenuate homocysteine induced neurotoxicity (Poddar and Paul, 2009; Poddar and Paul, 2013). These studies also showed that the signaling cascade downstream of ERK MAPK phosphorylation involves p38 MAPK dependent caspase-3 activation that eventually leads to neuronal cell death. Together, these findings provides a mechanistic basis for GluN2A-NMDAR dependent exacerbation of ischemic brain damage under hyperhomocysteinemic condition.

In conclusion, the present study provides the first direct evidence that mild hyperhomocysteinemia accelerates the progression of ischemic brain injury. The study also demonstrates that transient focal ischemia under hyperhomocysteinemic condition triggers two divergent pathogenic pathways resulting in exacerbation of brain injury. While activation of GluN2B-NMDARs contributes to glutamate-mediated ischemic brain injury, GluN2A-NMDAR stimulation plays a critical role in homocysteine-dependent brain damage. These unique findings not only establish that homocysteine-dependent neuronal injury and subsequent brain damage is distinctly different from the mechanisms generally implicated in ischemic brain injury but also highlights the differential response of NMDAR subtypes to homocysteine and glutamate in facilitating neurotoxicity. Thus, it appears that the view that GluN2B-NMDARs promotes apoptosis whereas GluN2A-NMDARs opposes apoptosis in neurons is overly simplistic, and detailed analysis of these pathways is warranted in any model of neurotoxicity.

ACKNOWLEDGEMENTS: We thank Dr. Yves Auberson for providing us with the pharmacological compound NVP-AAM077 and Dr. Andrew Holmes for coordinating and

providing us the GluN2A-knockout mice. We also thank Dr. Yirong Yang at the preclinical MRI core facility, BRaIN Imaging Center, UNM for performing the MRI scans and assistance with data analyses.

FUNDING: This work was supported by the National Institutes of Health grants RO1 NS083914 (Poddar, R) and RO1 NS059962 (Paul, S).

CONFLICT OF INTEREST: The authors declare no competing financial interests.

REFERENCES

- Auberson, Y. P., et al., 2002. 5-Phosphonomethylquinolinediones as competitive NMDA receptor antagonists with a preference for the human 1A/2A, rather than 1A/2B receptor composition. *Bioorg Med Chem Lett.* 12, 1099-102.
- Austin, R. C., et al., 2004. Role of hyperhomocysteinemia in endothelial dysfunction and atherothrombotic disease. *Cell Death Differ.* 11 Suppl 1, S56-64.
- Balkaya, M., et al., 2013. Assessing post-stroke behavior in mouse models of focal ischemia. *J Cereb Blood Flow Metab.* 33, 330-8.
- Barria, A., Malinow, R., 2002. Subunit-specific NMDA receptor trafficking to synapses. *Neuron.* 35, 345-53.
- Bouet, V., et al., 2009. The adhesive removal test: a sensitive method to assess sensorimotor deficits in mice. *Nat Protoc.* 4, 1560-4.
- Bouet, V., et al., 2007. Sensorimotor and cognitive deficits after transient middle cerebral artery occlusion in the mouse. *Exp Neurol.* 203, 555-67.
- Candelario-Jalil, E., et al., 2004. Wide therapeutic time window for nimesulide neuroprotection in a model of transient focal cerebral ischemia in the rat. *Brain Res.* 1007, 98-108.

- Chaperon, F., et al., 2003. Substitution for PCP, disruption of prepulse inhibition and hyperactivity induced by N-methyl-D-aspartate receptor antagonists: preferential involvement of the NR2B rather than NR2A subunit. *Behav Pharmacol.* 14, 477-87.
- Chen, C., et al., 2002. Intraperitoneal infusion of homocysteine increases intimal hyperplasia in balloon-injured rat carotid arteries. *Atherosclerosis.* 160, 103-14.
- Chen, M., et al., 2008. Differential roles of NMDA receptor subtypes in ischemic neuronal cell death and ischemic tolerance. *Stroke.* 39, 3042-8.
- Chen, S., Diamond, J. S., 2002. Synaptically released glutamate activates extrasynaptic NMDA receptors on cells in the ganglion cell layer of rat retina. *J Neurosci.* 22, 2165-73.
- Chin, J. H., Vora, N., 2014. The global burden of neurologic diseases. *Neurology.* 83, 349-51.
- Christie, L. A., et al., 2005. Enhanced hippocampal long-term potentiation in rats after chronic exposure to homocysteine. *Neurosci Lett.* 373, 119-24.
- Clark, B. A., Cull-Candy, S. G., 2002. Activity-dependent recruitment of extrasynaptic NMDA receptor activation at an AMPA receptor-only synapse. *J Neurosci.* 22, 4428-36.
- Clark, R. K., et al., 1993. Development of tissue damage, inflammation and resolution following stroke: an immunohistochemical and quantitative planimetric study. *Brain Res Bull.* 31, 565-72.
- Dalton, G. L., et al., 2012. NMDA GluN2A and GluN2B receptors play separate roles in the induction of LTP and LTD in the amygdala and in the acquisition and extinction of conditioned fear. *Neuropharmacology.* 62, 797-806.
- Dayal, S., et al., 2004. Cerebral vascular dysfunction mediated by superoxide in hyperhomocysteinemic mice. *Stroke.* 35, 1957-62.

- Dayal, S., Lentz, S. R., 2008. Murine models of hyperhomocysteinemia and their vascular phenotypes. *Arterioscler Thromb Vasc Biol.* 28, 1596-605.
- Deb, I., et al., 2013. Neuroprotective role of a brain-enriched tyrosine phosphatase, STEP, in focal cerebral ischemia. *J Neurosci.* 33, 17814-26.
- DeRidder, M. N., et al., 2006. Traumatic mechanical injury to the hippocampus in vitro causes regional caspase-3 and calpain activation that is influenced by NMDA receptor subunit composition. *Neurobiol Dis.* 22, 165-76.
- Devlin, A. M., et al., 2004. Effect of Mthfr genotype on diet-induced hyperhomocysteinemia and vascular function in mice. *Blood.* 103, 2624-9.
- Dingledine, R., et al., 1999. The glutamate receptor ion channels. *Pharmacol Rev.* 51, 7-61.
- Duan, W., et al., 2002. Dietary folate deficiency and elevated homocysteine levels endanger dopaminergic neurons in models of Parkinson's disease. *J Neurochem.* 80, 101-10.
- Dunham, N. W., Miya, T. S., 1957. A note on a simple apparatus for detecting neurological deficit in rats and mice. *J Am Pharm Assoc Am Pharm Assoc.* 46, 208-9.
- Endres, M., et al., 2005. Folate deficiency increases postischemic brain injury. *Stroke.* 36, 321-5.
- Fischer, G., et al., 1997. Ro 25-6981, a highly potent and selective blocker of N-methyl-D-aspartate receptors containing the NR2B subunit. Characterization in vitro. *J Pharmacol Exp Ther.* 283, 1285-92.
- Fisher, M., et al., 2009. Update of the stroke therapy academic industry roundtable preclinical recommendations. *Stroke.* 40, 2244-50.
- Foster, K. A., et al., 2010. Distinct roles of NR2A and NR2B cytoplasmic tails in long-term potentiation. *J Neurosci.* 30, 2676-85.

- Fox, C. J., et al., 2006. Contribution of NR2A and NR2B NMDA subunits to bidirectional synaptic plasticity in the hippocampus in vivo. *Hippocampus*. 16, 907-15.
- Ganapathy, P. S., et al., 2011. The role of N-methyl-D-aspartate receptor activation in homocysteine-induced death of retinal ganglion cells. *Invest Ophthalmol Vis Sci*. 52, 5515-24.
- Gilfix, B. M., et al., 1997. Novel reductant for determination of total plasma homocysteine. *Clin Chem*. 43, 687-8.
- Gladding, C. M., Raymond, L. A., 2011. Mechanisms underlying NMDA receptor synaptic/extrasynaptic distribution and function. *Mol Cell Neurosci*. 48, 308-20.
- Gogas, K. R., 2006. Glutamate-based therapeutic approaches: NR2B receptor antagonists. *Curr Opin Pharmacol*. 6, 68-74.
- Hankey, G. J., Eikelboom, J. W., 2001. Homocysteine and stroke. *Curr Opin Neurol*. 14, 95-102.
- Hardingham, G. E., Bading, H., 2003. The Yin and Yang of NMDA receptor signalling. *Trends Neurosci*. 26, 81-9.
- Hardingham, G. E., Bading, H., 2010. Synaptic versus extrasynaptic NMDA receptor signalling: implications for neurodegenerative disorders. *Nat Rev Neurosci*. 11, 682-96.
- Hardingham, G. E., et al., 2002. Extrasynaptic NMDARs oppose synaptic NMDARs by triggering CREB shut-off and cell death pathways. *Nat Neurosci*. 5, 405-14.
- Harris, A. Z., Pettit, D. L., 2007. Extrasynaptic and synaptic NMDA receptors form stable and uniform pools in rat hippocampal slices. *J Physiol*. 584, 509-19.
- Harris, A. Z., Pettit, D. L., 2008. Recruiting extrasynaptic NMDA receptors augments synaptic signaling. *J Neurophysiol*. 99, 524-33.

- Jacobsen, D. W., et al., 1994. Rapid HPLC determination of total homocysteine and other thiols in serum and plasma: sex differences and correlation with cobalamin and folate concentrations in healthy subjects. *Clin Chem.* 40, 873-81.
- Janson, J. J., et al., 2002. Prevalence of hyperhomocysteinemia in an elderly population. *Am J Hypertens.* 15, 394-7.
- Jara-Prado, A., et al., 2003. Homocysteine-induced brain lipid peroxidation: effects of NMDA receptor blockade, antioxidant treatment, and nitric oxide synthase inhibition. *Neurotox Res.* 5, 237-43.
- Johansen-Berg, H., Behrens, T. E. J., 2014. *Diffusion MRI : from quantitative measurement to in-vivo neuroanatomy.* Elsevier/Academic Press, London, UK ; Waltham, MA.
- Johnston, S. C., et al., 2009. Global variation in stroke burden and mortality: estimates from monitoring, surveillance, and modelling. *Lancet Neurol.* 8, 345-54.
- Kalani, A., et al., 2014. Nutri-epigenetics ameliorates blood-brain barrier damage and neurodegeneration in hyperhomocysteinemia: role of folic acid. *J Mol Neurosci.* 52, 202-15.
- Kamath, A. F., et al., 2006. Elevated levels of homocysteine compromise blood-brain barrier integrity in mice. *Blood.* 107, 591-3.
- Kim, M. J., et al., 2005. Differential roles of NR2A- and NR2B-containing NMDA receptors in Ras-ERK signaling and AMPA receptor trafficking. *Neuron.* 46, 745-60.
- Knight, R. A., et al., 1991. Temporal evolution of ischemic damage in rat brain measured by proton nuclear magnetic resonance imaging. *Stroke.* 22, 802-8.
- Kruman, II, et al., 2000. Homocysteine elicits a DNA damage response in neurons that promotes apoptosis and hypersensitivity to excitotoxicity. *J Neurosci.* 20, 6920-6.

- Kruman, II, et al., 2002. Folic acid deficiency and homocysteine impair DNA repair in hippocampal neurons and sensitize them to amyloid toxicity in experimental models of Alzheimer's disease. *J Neurosci.* 22, 1752-62.
- Lai, T. W., et al., 2011. Stroke intervention pathways: NMDA receptors and beyond. *Trends Mol Med.* 17, 266-75.
- Li, B., et al., 2002. Differential regulation of synaptic and extra-synaptic NMDA receptors. *Nat Neurosci.* 5, 833-4.
- Li, H., et al., 2014. Histological, cellular and behavioral assessments of stroke outcomes after photothrombosis-induced ischemia in adult mice. *BMC Neurosci.* 15, 58.
- Li, X., et al., 2004. Chronic behavioral testing after focal ischemia in the mouse: functional recovery and the effects of gender. *Exp Neurol.* 187, 94-104.
- Lipton, S. A., et al., 1997. Neurotoxicity associated with dual actions of homocysteine at the N-methyl-D-aspartate receptor. *Proc Natl Acad Sci U S A.* 94, 5923-8.
- Liu, L., et al., 2004. Role of NMDA receptor subtypes in governing the direction of hippocampal synaptic plasticity. *Science.* 304, 1021-4.
- Liu, Y., et al., 2013. Quantitative gait analysis of long-term locomotion deficits in classical unilateral striatal intracerebral hemorrhage rat model. *Behav Brain Res.* 257, 166-77.
- Liu, Y., et al., 2007. NMDA receptor subunits have differential roles in mediating excitotoxic neuronal death both in vitro and in vivo. *J Neurosci.* 27, 2846-57.
- Longa, E. Z., et al., 1989. Reversible middle cerebral artery occlusion without craniectomy in rats. *Stroke.* 20, 84-91.
- Lozovaya, N. A., et al., 2004. Extrasynaptic NR2B and NR2D subunits of NMDA receptors shape 'superslow' afterburst EPSC in rat hippocampus. *J Physiol.* 558, 451-63.

- Lynch, D. R., Guttman, R. P., 2002. Excitotoxicity: perspectives based on N-methyl-D-aspartate receptor subtypes. *J Pharmacol Exp Ther.* 300, 717-23.
- Martel, M. A., et al., 2012. The subtype of GluN2 C-terminal domain determines the response to excitotoxic insults. *Neuron.* 74, 543-56.
- Massey, P. V., et al., 2004. Differential roles of NR2A and NR2B-containing NMDA receptors in cortical long-term potentiation and long-term depression. *J Neurosci.* 24, 7821-8.
- McCully, K. S., 2007. Homocysteine, vitamins, and vascular disease prevention. *Am J Clin Nutr.* 86, 1563S-8S.
- Michinaga, S., Koyama, Y., 2015. Pathogenesis of brain edema and investigation into anti-edema drugs. *Int J Mol Sci.* 16, 9949-75.
- Miller, J. W., et al., 2013. Homocysteine, cysteine, and risk of incident colorectal cancer in the Women's Health Initiative observational cohort. *Am J Clin Nutr.* 97, 827-34.
- Morikawa, E., et al., 1998. Attenuation of focal ischemic brain injury in mice deficient in the epsilon1 (NR2A) subunit of NMDA receptor. *J Neurosci.* 18, 9727-32.
- Morita, H., et al., 2001. Diet-induced hyperhomocysteinemia exacerbates neointima formation in rat carotid arteries after balloon injury. *Circulation.* 103, 133-9.
- Mukaka, M. M., 2012. Statistics corner: A guide to appropriate use of correlation coefficient in medical research. *Malawi Med J.* 24, 69-71.
- Mutel, V., et al., 1998. In vitro binding properties in rat brain of [3H]Ro 25-6981, a potent and selective antagonist of NMDA receptors containing NR2B subunits. *J Neurochem.* 70, 2147-55.

- Obeid, R., Herrmann, W., 2006. Mechanisms of homocysteine neurotoxicity in neurodegenerative diseases with special reference to dementia. *FEBS Lett.* 580, 2994-3005.
- Papadia, S., et al., 2005. Nuclear Ca^{2+} and the cAMP response element-binding protein family mediate a late phase of activity-dependent neuroprotection. *J Neurosci.* 25, 4279-87.
- Papouin, T., Oliet, S. H., 2014. Organization, control and function of extrasynaptic NMDA receptors. *Philos Trans R Soc Lond B Biol Sci.* 369, 20130601.
- Parkkinen, S., et al., 2013. Gait impairment in a rat model of focal cerebral ischemia. *Stroke Res Treat.* 2013, 410972.
- Parsons, C. G., et al., 1998. Glutamate in CNS disorders as a target for drug development: an update. *Drug News Perspect.* 11, 523-69.
- Petralia, R. S., et al., 2010. Organization of NMDA receptors at extrasynaptic locations. *Neuroscience.* 167, 68-87.
- Pitkonen, M., et al., 2012. Long-term evolution of diffusion tensor indices after temporary experimental ischemic stroke in rats. *Brain Res.* 1445, 103-10.
- Poddar, R., et al., 2017a. Role of AMPA receptors in homocysteine-NMDA receptor-induced crosstalk between ERK and p38 MAPK. *J Neurochem.* 142, 560-573.
- Poddar, R., Paul, S., 2009. Homocysteine-NMDA receptor-mediated activation of extracellular signal-regulated kinase leads to neuronal cell death. *J Neurochem.* 110, 1095-106.
- Poddar, R., Paul, S., 2013. Novel crosstalk between ERK MAPK and p38 MAPK leads to homocysteine-NMDA receptor-mediated neuronal cell death. *J Neurochem.* 124, 558-70.

- Poddar, R., et al., 2017b. A peptide mimetic of tyrosine phosphatase STEP as a potential therapeutic agent for treatment of cerebral ischemic stroke. *J Cereb Blood Flow Metab.* 271678X17747193.
- Poddar, R., et al., 2001. Homocysteine induces expression and secretion of monocyte chemoattractant protein-1 and interleukin-8 in human aortic endothelial cells: implications for vascular disease. *Circulation.* 103, 2717-23.
- Ramos, M. I., et al., 2005. Low folate status is associated with impaired cognitive function and dementia in the Sacramento Area Latino Study on Aging. *Am J Clin Nutr.* 82, 1346-52.
- Refsum, H., et al., 1998. Homocysteine and cardiovascular disease. *Annu Rev Med.* 49, 31-62.
- Rewell, S. S., et al., 2017. Evolution of ischemic damage and behavioural deficit over 6 months after MCAo in the rat: Selecting the optimal outcomes and statistical power for multi-centre preclinical trials. *PLoS One.* 12, e0171688.
- Riccio, A., Ginty, D. D., 2002. What a privilege to reside at the synapse: NMDA receptor signaling to CREB. *Nat Neurosci.* 5, 389-90.
- Robles, N. R., et al., 2005. Hyperhomocysteinemia in patients with mild chronic renal failure. *Eur J Intern Med.* 16, 334-8.
- Sakimura, K., et al., 1995. Reduced hippocampal LTP and spatial learning in mice lacking NMDA receptor epsilon 1 subunit. *Nature.* 373, 151-5.
- Schaar, K. L., et al., 2010. Functional assessments in the rodent stroke model. *Exp Transl Stroke Med.* 2, 13.
- Schaefer, P. W., et al., 2000. Diffusion-weighted MR imaging of the brain. *Radiology.* 217, 331-45.

- Schumann, J., et al., 2008. Inhibition of NR2B phosphorylation restores alterations in NMDA receptor expression and improves functional recovery following traumatic brain injury in mice. *J Neurotrauma*. 25, 945-57.
- Scinemi, A., et al., 2004. NR2B-containing receptors mediate cross talk among hippocampal synapses. *J Neurosci*. 24, 4767-77.
- Selhub, J., et al., 1999. Serum total homocysteine concentrations in the third National Health and Nutrition Examination Survey (1991-1994): population reference ranges and contribution of vitamin status to high serum concentrations. *Ann Intern Med*. 131, 331-9.
- Seshadri, S., et al., 2002. Plasma homocysteine as a risk factor for dementia and Alzheimer's disease. *N Engl J Med*. 346, 476-83.
- Shen, J. M., et al., 2011. The use of MRI apparent diffusion coefficient (ADC) in monitoring the development of brain infarction. *BMC Med Imaging*. 11, 2.
- Sibarov, D. A., et al., 2016. GluN2A Subunit-Containing NMDA Receptors Are the Preferential Neuronal Targets of Homocysteine. *Front Cell Neurosci*. 10, 246.
- Sood, R., et al., 2009. Increased apparent diffusion coefficients on MRI linked with matrix metalloproteinases and edema in white matter after bilateral carotid artery occlusion in rats. *J Cereb Blood Flow Metab*. 29, 308-16.
- Soriano, F. X., et al., 2008. Specific targeting of pro-death NMDA receptor signals with differing reliance on the NR2B PDZ ligand. *J Neurosci*. 28, 10696-710.
- Sotak, C. H., 2002. The role of diffusion tensor imaging in the evaluation of ischemic brain injury - a review. *NMR Biomed*. 15, 561-9.
- Swanson, R. A., et al., 1990. A semiautomated method for measuring brain infarct volume. *J Cereb Blood Flow Metab*. 10, 290-3.

- Taheri, S., Sood, R., 2007. Partial volume effect compensation for improved reliability of quantitative blood-brain barrier permeability. *Magn Reson Imaging*. 25, 613-25.
- Takamatsu, H., et al., 2002. Time courses of progress to the chronic stage of middle cerebral artery occlusion models in rats. *Exp Brain Res*. 146, 95-102.
- Terasaki, Y., et al., 2010. Activation of NR2A receptors induces ischemic tolerance through CREB signaling. *J Cereb Blood Flow Metab*. 30, 1441-9.
- Tigaret, C. M., et al., 2006. Subunit dependencies of N-methyl-D-aspartate (NMDA) receptor-induced alpha-amino-3-hydroxy-5-methyl-4-isoxazolepropionic acid (AMPA) receptor internalization. *Mol Pharmacol*. 69, 1251-9.
- Tovar, K. R., Westbrook, G. L., 1999. The incorporation of NMDA receptors with a distinct subunit composition at nascent hippocampal synapses in vitro. *J Neurosci*. 19, 4180-8.
- Tu, W., et al., 2010. DAPK1 interaction with NMDA receptor NR2B subunits mediates brain damage in stroke. *Cell*. 140, 222-34.
- Ungvari, Z., et al., 1999. Dysfunction of nitric oxide mediation in isolated rat arterioles with methionine diet-induced hyperhomocysteinemia. *Arterioscler Thromb Vasc Biol*. 19, 1899-904.
- Vicini, S., et al., 1998. Functional and pharmacological differences between recombinant N-methyl-D-aspartate receptors. *J Neurophysiol*. 79, 555-66.
- Virley, D., et al., 2000. A temporal MRI assessment of neuropathology after transient middle cerebral artery occlusion in the rat: correlations with behavior. *J Cereb Blood Flow Metab*. 20, 563-82.
- Wang, J., et al., 2003. Cdk5 activation induces hippocampal CA1 cell death by directly phosphorylating NMDA receptors. *Nat Neurosci*. 6, 1039-47.

- Wang, Y., et al., 2008. A comprehensive analysis of gait impairment after experimental stroke and the therapeutic effect of environmental enrichment in rats. *J Cereb Blood Flow Metab.* 28, 1936-50.
- Yang, Y., et al., 2013. Early inhibition of MMP activity in ischemic rat brain promotes expression of tight junction proteins and angiogenesis during recovery. *J Cereb Blood Flow Metab.* 33, 1104-14.
- Zhang, C., et al., 2010. NMDA receptor-mediated activation of NADPH oxidase and glomerulosclerosis in hyperhomocysteinemic rats. *Antioxid Redox Signal.* 13, 975-86.
- Zhang, S. J., et al., 2007. Decoding NMDA receptor signaling: identification of genomic programs specifying neuronal survival and death. *Neuron.* 53, 549-62.
- Zhou, X., et al., 2013. Involvement of the GluN2A and GluN2B subunits in synaptic and extrasynaptic N-methyl-D-aspartate receptor function and neuronal excitotoxicity. *J Biol Chem.* 288, 24151-9.
- Zoccolella, S., et al., 2006. Hyperhomocysteinemia in movement disorders: Current evidence and hypotheses. *Curr Vasc Pharmacol.* 4, 237-43.

FIGURE LEGENDS

Figure 1. Evaluation of total plasma homocysteine levels in hyperhomocysteinemic rats by HPLC. (A) Schematic representation of the timeline of implantation of saline or homocysteine containing osmotic pumps and blood collection. (B) Quantitative analysis of total plasma homocysteine levels in rats implanted with saline (control) or homocysteine (HHcy) pumps, before (0 day) and after (3, 5 and 7 days) pump implantation. Values expressed as mean \pm SEM (control: n = 4-9, HHcy: n = 7-10). *p < 0.0001 for control vs. HHcy rats.

Figure 2. Exacerbation of ischemic brain damage in hyperhomocysteinemic rats at 24h post-occlusion evaluated from T2 maps. (A) Schematic representation of the timeline of implantation of osmotic pumps, MCAO, MRI scans and behavioral assessments. (B) Quantitative analysis of stroke mortality rate (%) in control and hyperhomocysteinemic (HHcy) rats. (C) Representative T2 maps acquired from sham control and HHcy rats, as well as control and HHcy rats subjected to MCAO (60 min) and reperfusion (24h). (D) Quantitative analysis of ischemic lesion volume in control and HHcy rats subjected to ischemic insult and reperfusion, expressed as mean \pm SEM (control: n = 11, HHcy: n = 15); *p < 0.0001 for control vs. HHcy rats.

Figure 3. Temporal evolution of ischemic brain damage in hyperhomocysteinemic rats evaluated from T2, ADC and FA maps. (A) Representative T2 maps from days 1, 3 and 14 after MCAO, acquired from control and hyperhomocysteinemic rats (HHcy) showing changes in ischemic lesion size from rostral to caudal regions of the brain. Corresponding bar diagram provide quantitative analysis of total infarct volume, expressed as mean \pm SEM (on day 1 and 3 - control: n = 11, HHcy: n = 15; on day 14 - control: n = 10, HHcy: n = 14). (B) Representative ADC maps acquired from control and HHcy rats at day 14 post-MCAO featuring hyperintense areas that co-localize with the lesion area in the T2 maps at day 14 post-MCAO. Quantitative analysis of ADC values in the lesion area, expressed as mean \pm SEM (control: n = 10, HHcy: n = 14). (C) Representative FA maps acquired from the same slices as ADC and T2 maps at 14 days post-MCAO as well as quantitative analysis of FA values expressed as mean \pm SEM (control: n = 10, HHcy: n = 14). (D) Representative cresyl violet stained images of rostral and caudal

regions of the brain from control and HHcy rats 14 days after MCAO. * $p < 0.05$, ** $p < 0.01$ and *** $p < 0.001$ for control vs. HHcy rats.

Figure 4. Pharmacological inhibition of GluN2A-NMDAR with NVP-AAM077 attenuates hyperhomocysteinemia-induced exacerbation of ischemic brain damage. (A) Representative T2 maps at 24h post-MCAO acquired from control and hyperhomocysteinemic (HHcy) rats treated with vehicle, NVP-AAM077 (NVP) or Ro 256981 at the onset of the ischemic insult. (B - D) Quantitative analysis of total infarct volume in (B, D) control rats treated with NVP or Ro 256981; and (C, E) HHcy rats treated with NVP or Ro 256981. Values are expressed as mean \pm SEM (control: $n = 11$, control + NVP: $n = 12$, vehicle + Ro 256981: $n = 10$, HHcy: $n = 15$, HHcy + NVP: $n = 11$, HHcy + Ro256981: $n = 7$). * $p < 0.005$ for control vs. control + Ro 256981 treated rats and ** $p < 0.001$ for HHcy vs. HHcy + NVP treated rats.

Figure 5. Effect of GluN2A-NMDARs inhibition on the progression of ischemic brain damage in hyperhomocysteinemic rats. (A) Representative T2 maps from days 1, 3 and 14 after MCAO, acquired from hyperhomocysteinemic rats treated with vehicle (HHcy) or NVP-AAM077 (HHcy + NVP), showing changes in ischemic lesion size from rostral to caudal regions of the brain. Corresponding bar diagram provide quantitative analysis of total infarct volume, expressed as mean \pm SEM (on days 1 and 3 - HHcy: $n = 15$; on day 14 - HHcy: $n = 14$; on days 1, 3 and 14 - HHcy + NVP: $n = 11$). (B) Representative ADC maps acquired from HHcy and HHcy + NVP treated rats at day 14 post-MCAO, featuring hyperintense areas that co-localize with the lesion area in the T2 maps at day 14 post-MCAO. Quantitative analysis of ADC values in the lesion area, expressed as mean \pm SEM (HHcy: $n = 14$, HHcy + NVP: $n = 10$). (C)

Representative FA maps acquired from the same slices as ADC and T2 maps at 14 days post-MCAO as well as quantitative analysis of FA values expressed as mean \pm SEM (HHcy: n = 14, HHcy + NVP: n = 10). *p < 0.01, **p < 0.005 and ***p < 0.001 for HHcy vs. HHcy + NVP treated rats.

Figure 6. Effect of GluN2A-NMDAR inhibition on ischemia-induced normal gait impairment, motor coordination and sensorimotor deficit in hyperhomocysteinemic rats.

(A-G) Control, hyperhomocysteinemic (HHcy) and hyperhomocysteinemic rats treated with GluN2A-NMDAR inhibitor NVP-AAM077 (HHcy + NVP) were subjected to MCAO followed by reperfusion. Quantitative analysis of (A) Maximum contact area (mm²); (B) Print area (mm²) and (C) Print position (cm) in the affected forepaw (contralateral) assessed by CatWalk 7 days after MCAO (control: n = 11, HHcy: n = 14, HHcy + NVP: n = 11). Quantitative analysis of (D) spontaneous contralateral forelimb use assessed using cylinder test (day 8 post MCAO; control: n = 7, HHcy: n = 14, HHcy + NVP: n = 11); (E) motor impairment and balance assessed using the rotarod test (day 8 post MCAO; control: n = 12, HHcy: n = 14, HHcy + NVP: n = 11); (F, G) mean latency to detect (F) and remove (G) an adhesive label from the contralateral forepaw (time in seconds) assessed as a measure of sensorimotor function (day 9 post MCAO; control: n = 12, HHcy: n = 15, HHcy + NVP: n = 11). All data are expressed as mean \pm SEM; *p < 0.05 and **p < 0.001 for control vs. HHcy rats; and #p < 0.05 and ##p < 0.001 for HHcy vs. HHcy + NVP treated rats.

Figure 7. Effect of GluN2A-NMDAR gene deletion on the exacerbation of ischemic brain damage in hyperhomocysteinemic mice. (A) Schematic representation of the timeline of blood

collection following implantation of osmotic pump, MCAO, reperfusion and MRI scan in wild-type (WT) and GluN2A-KO mice. (B) Quantitative analysis of total plasma homocysteine level in WT and hyperhomocysteinemic (HHcy) mice before (0 day) and after (3 and 5 days) implantation of pump. Values are expressed as mean \pm SEM (n = 3-5 / group); (C) Representative photomicrographs of T2 maps acquired from control-WT, HHcy-WT, control-GluN2A-KO and HHcy-GluN2A-KO mice following MCAO (30 min) and reperfusion (24h). (D) Quantitative analysis of total infarct volume in WT (control and HHcy) and GluN2A-KO (control or HHcy) mice. Values are expressed as mean \pm SEM (control-WT: n = 8, HHcy-WT: n = 5, control-GluN2A-KO: n = 3, HHcy-GluN2A-KO: n = 3). *p < 0.01 for WT mice day 0 vs. WT mice day 3 or 5; #p < 0.01 for GluN2A-KO mice day 0 vs. GluN2A-KO mice day 3 or 5. **p < 0.001 for control-WT vs. HHcy-WT mice.

Figure 8. Role of GluN2A-NMDAR in neuronal ERK MAPK phosphorylation and cell death following OGD in the presence of L-homocysteine. (A) Neuron cultures from embryonic rat brain were treated with 50 μ M L-homocysteine (L-Hcy) for 4h in the absence or presence of NVP-AAM077 (30 nM, left panel) or Ro 25-6981 (1 μ M, right panel). (B) Neuron cultures from WT and GluN2A KO mice embryonic brain were treated with 50 μ M L-Hcy for 4h. (C - E) Neuron cultures from embryonic rat brain were exposed to (C) OGD for specified time periods in the absence (left panel) or presence of L-Hcy (50 μ M, right panel); (D) OGD, OGD in the presence of L-Hcy (50 μ M) or OGD in the presence of L-Hcy and NVP-AAM077 (30 nM) for 3h; (E) OGD or OGD in the presence of L-Hcy (50 μ M) for 2h, followed by reoxygenation (ReOx) for 22h. (A-D) Immunoblot analysis of neuronal lysates using anti-phospho ERK MAPK antibody (pERK) and then reprobod with anti-ERK MAPK antibody (ERK). The

extent of ERK MAPK phosphorylation was quantified using computer-assisted densitometry and Image J analysis. Values are mean \pm SEM (n = 5). (A, C, D) *p < 0.001 from control and #p < 0.001 from 4 hr homocysteine treatment; (B) *p < 0.001 from corresponding controls of WT and GluN2A-NMDAR KO cultures. (E) Quantitative analysis of percentage of neurons with pyknotic nuclei following Hoechst DNA staining. Values are mean \pm SEM (n = 1500 cells / condition from 4 experiments). *p < 0.001 from control and #p < 0.001 from OGD/ReOx.

Figure 9. Role of GluN2A-NMDAR in ERK MAPK phosphorylation in hyperhomocysteinemic rats following MCAO (A) Control and hyperhomocysteinemic (HHcy) rats were subjected to MCAO for 60 min followed by reperfusion for the specified time periods (sham, 0, 3, 6, 12h). (B) Control, HHcy and HHcy rats treated with NVP-AAM077 (HHcy + NVP) were subjected to MCAO for 60 min followed by reperfusion for 3h. (A, B) Cortical tissue lysates from the ipsilateral hemisphere were analyzed by immunoblotting using anti-pERK and anti-ERK antibodies. The extent of ERK MAPK phosphorylation was quantified using computer-assisted densitometry and Image J analysis. Values are mean \pm SEM (n = 5). *p < 0.001 from corresponding control; and #p < 0.001 from HHcy.

HIGHLIGHTS

- Hyperhomocysteinemia (HHcy) exacerbate ischemic brain injury and functional deficit.
- Pharmacological inhibition of GluN2A-NMDAR reduces severity of ischemic brain injury in HHcy rats.
- GluN2A-NMDAR inhibition also reduces ischemia-induced functional deficits in HHcy rats.
- HHcy in GluN2A-NMDAR knockout mice fails to exacerbate ischemic brain injury.
- Study reveals a key role of GluN2A-NMDAR in neurodegeneration under HHcy condition.

ACCEPTED MANUSCRIPT

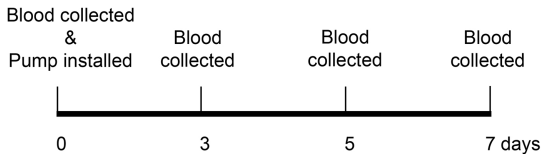
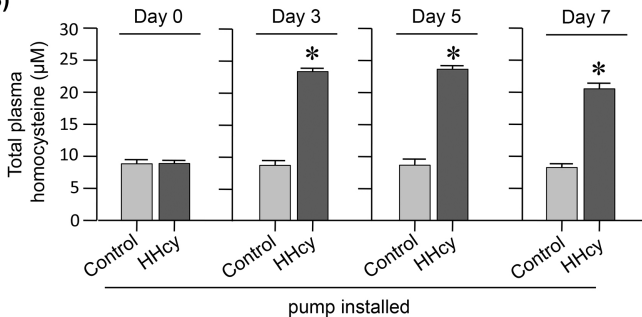
A)**B)**

Figure 1

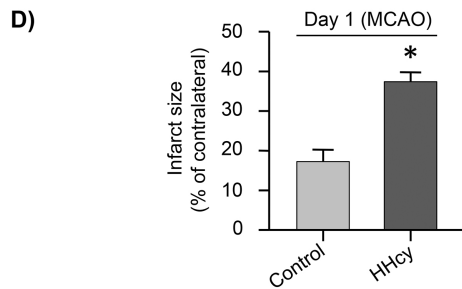
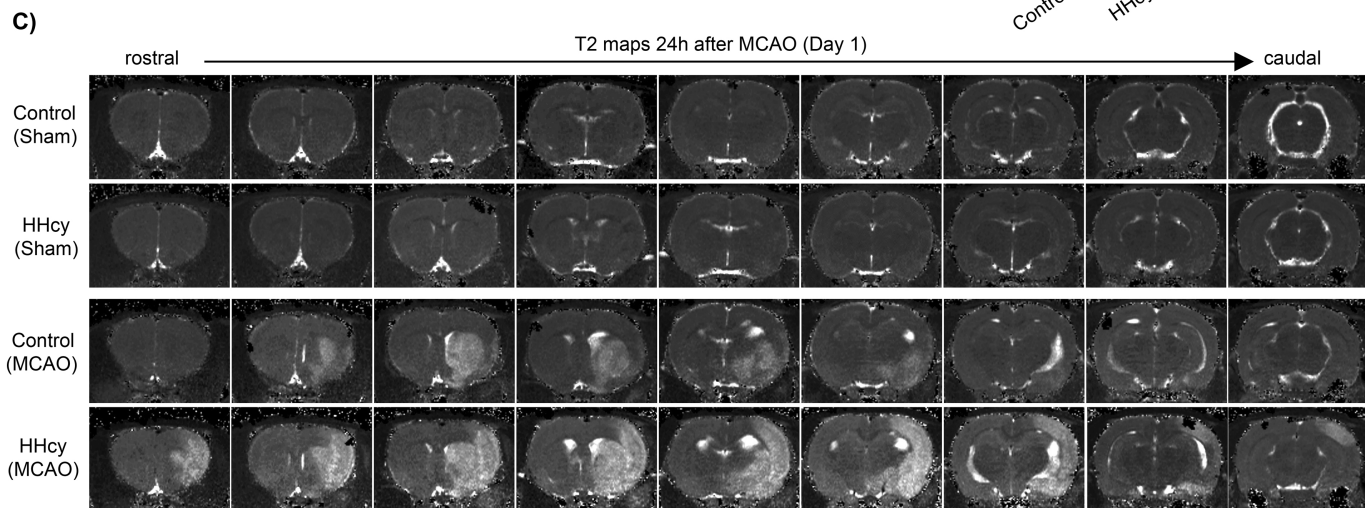
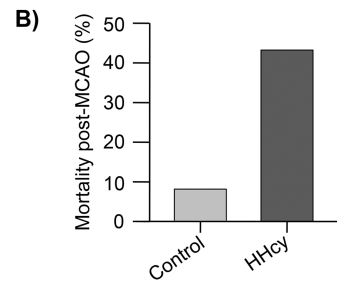
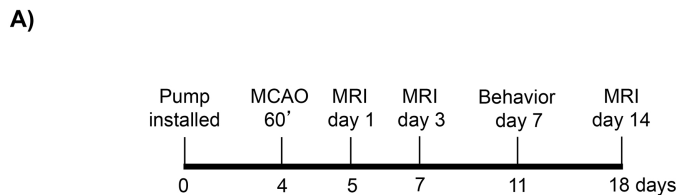


Figure 2

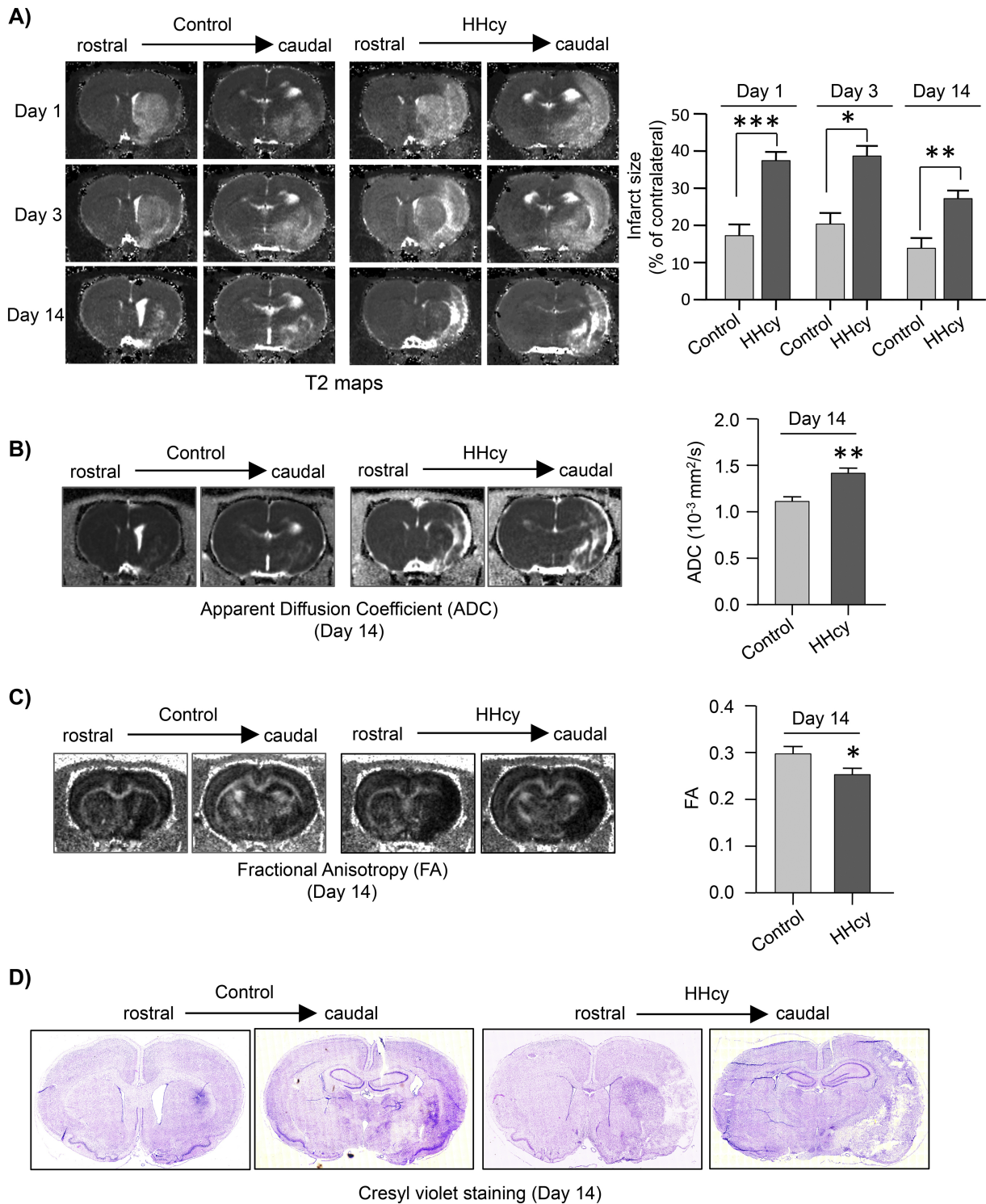


Figure 3

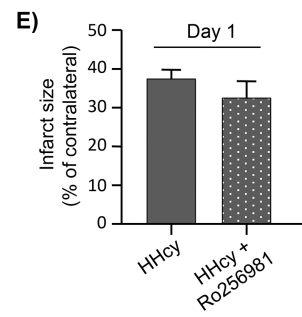
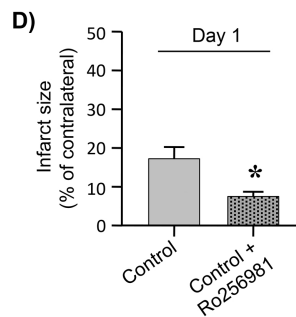
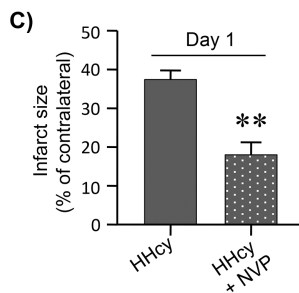
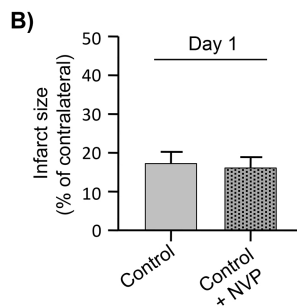
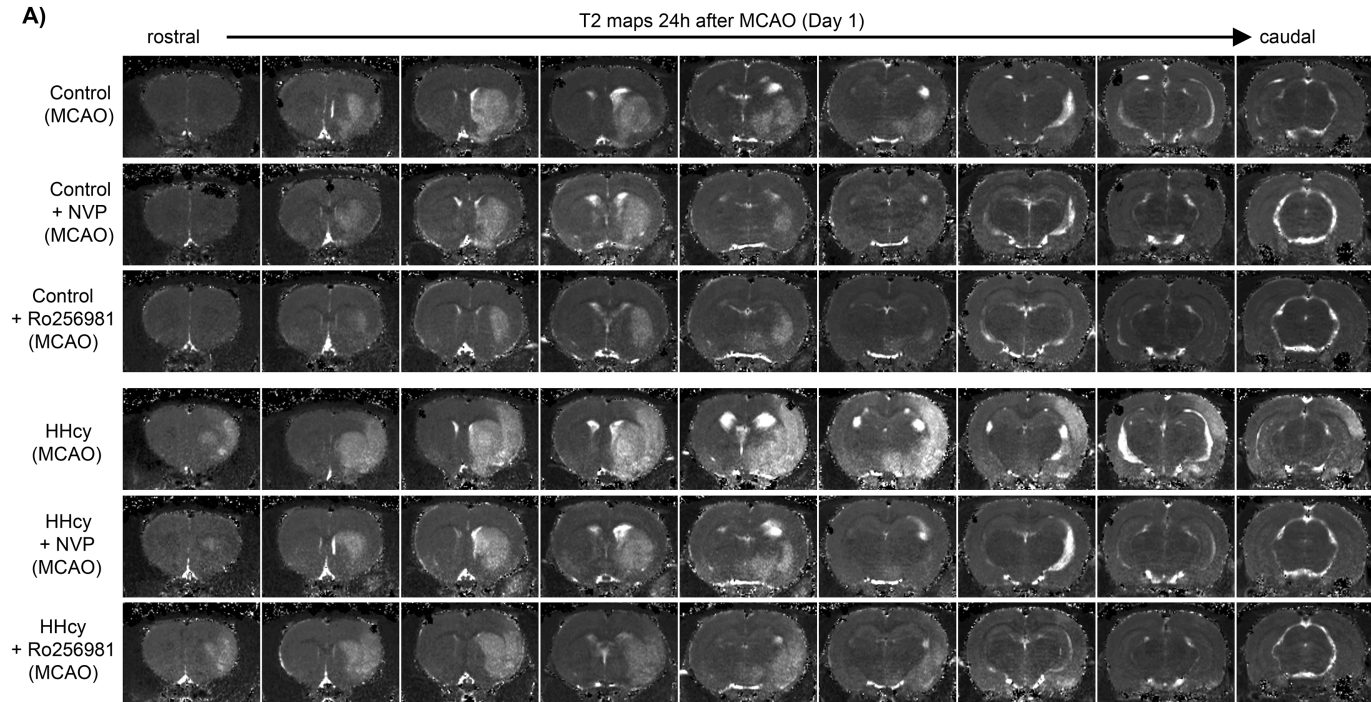


Figure 4

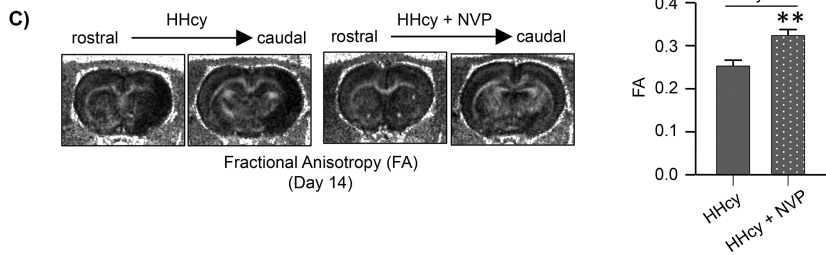
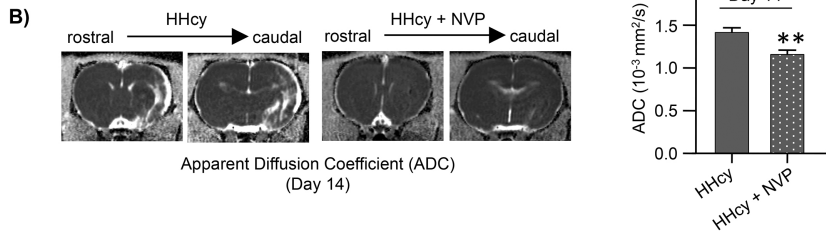
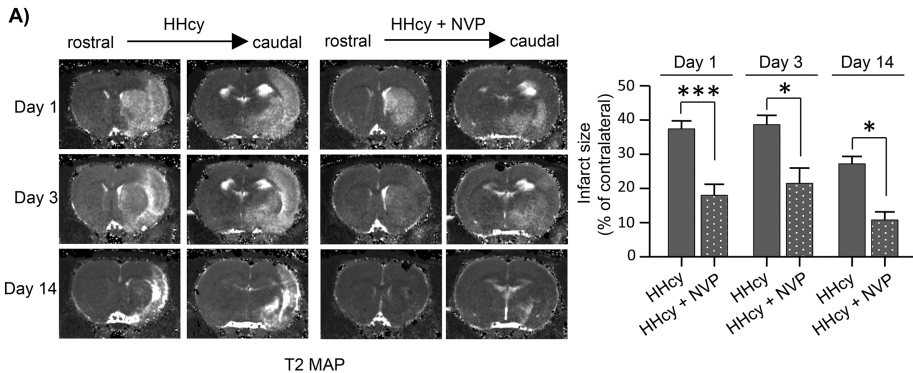


Figure 5

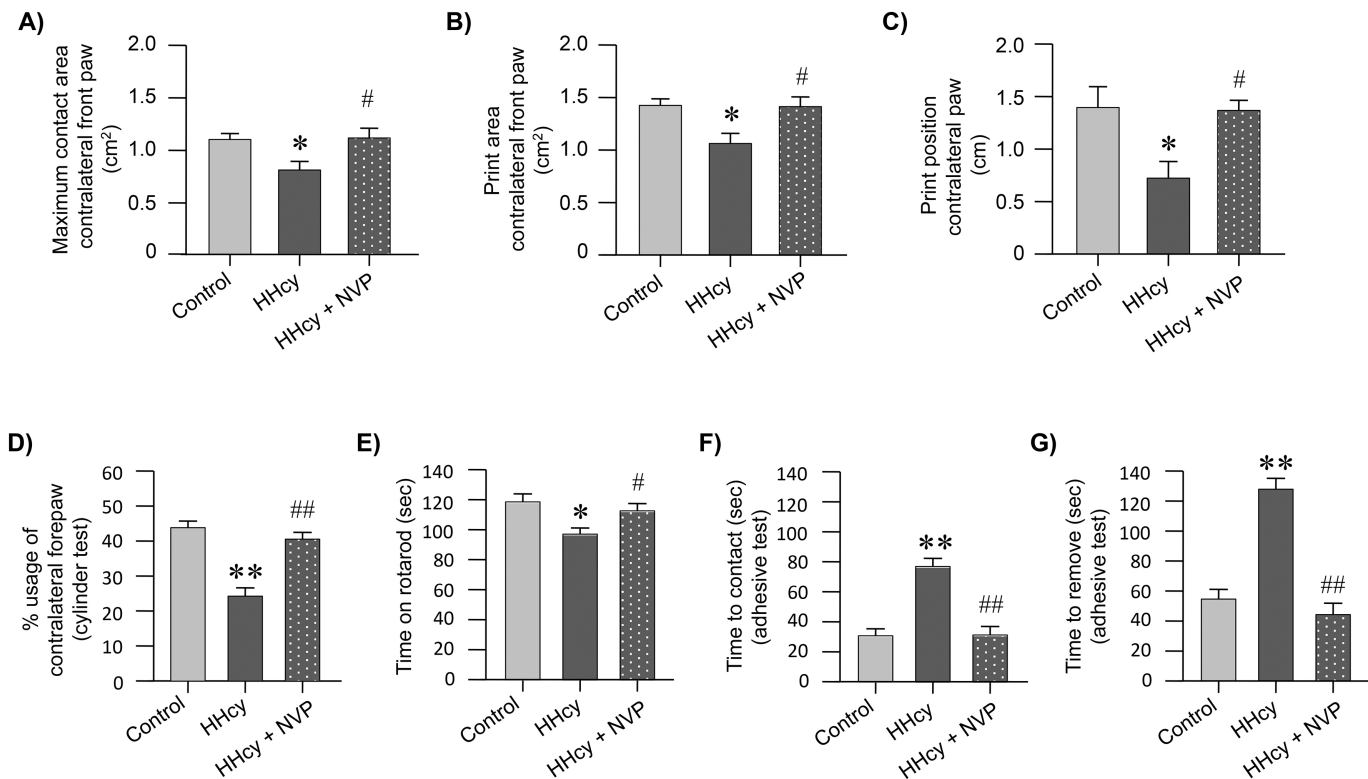


Figure 6

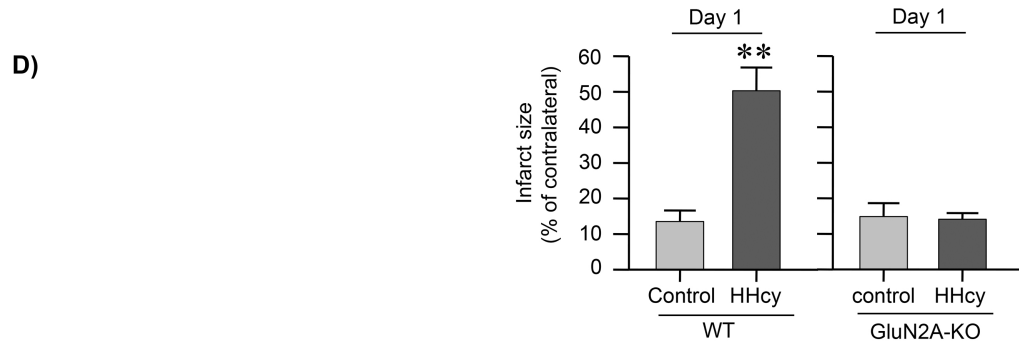
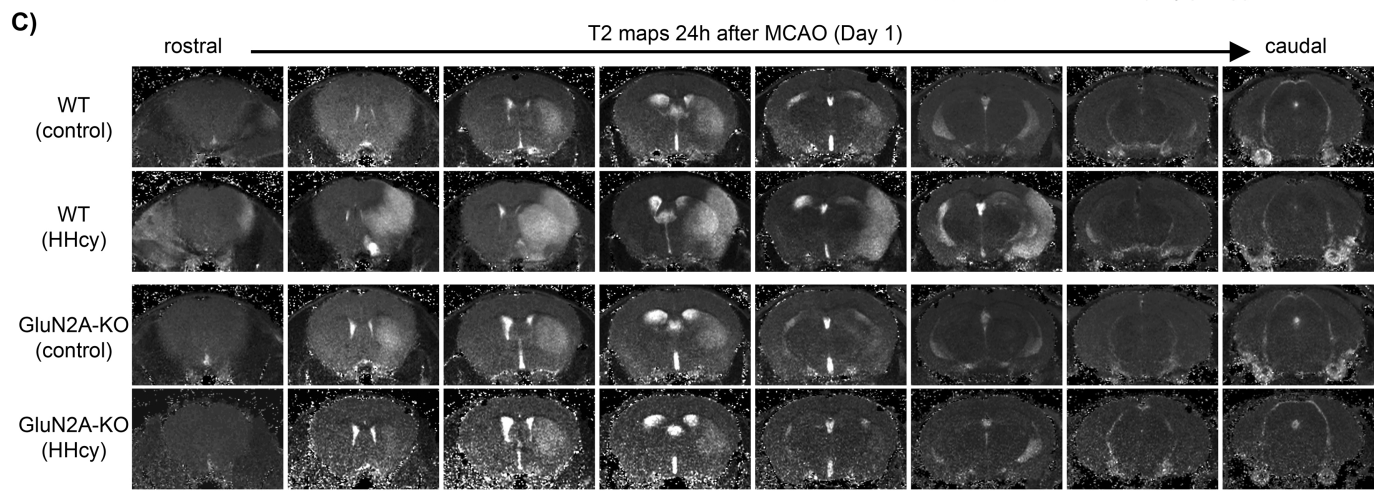
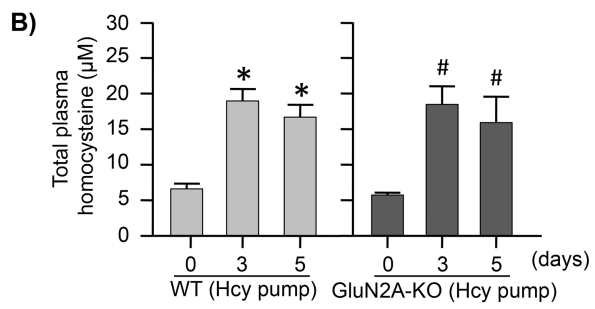
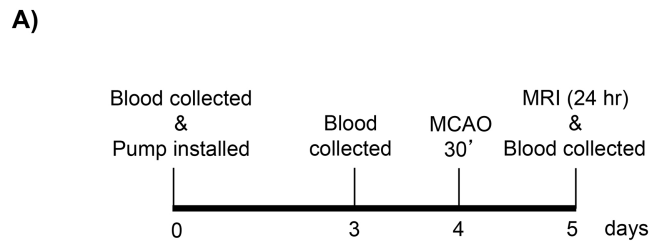


Figure 7

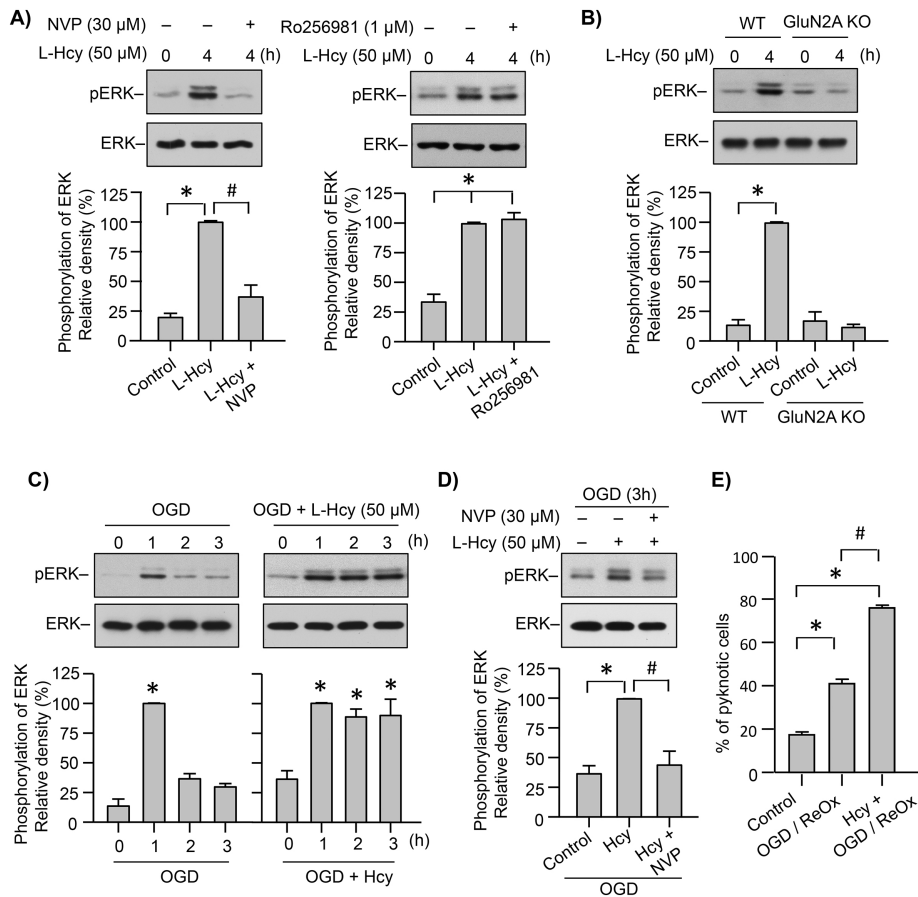


Figure 8

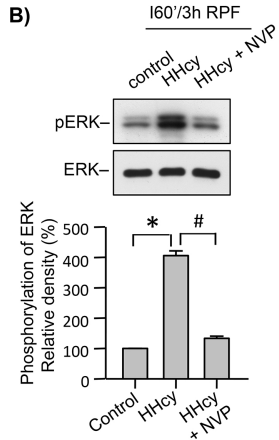
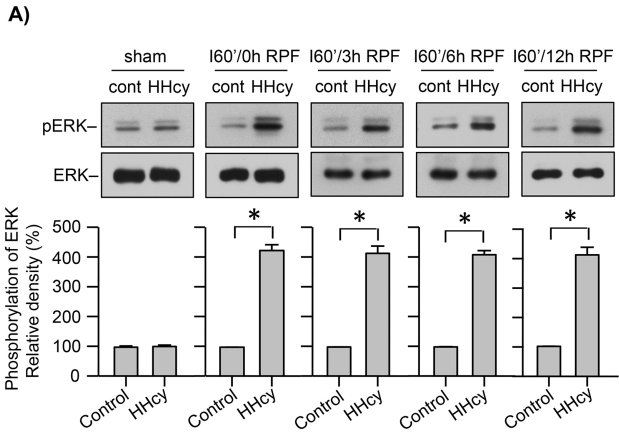


Figure 9